JACS

Electron Paramagnetic Resonance Signature of Tetragonal Low Spin Iron(V)-Nitrido and -Oxo Complexes Derived from the Electronic Structure Analysis of Heme and Non-Heme Archetypes

Hao-Ching Chang,[†,‡] Bhaskar Mondal,[§,‡] Huayi Fang,[§,⊥] Frank Neese,[†] Eckhard Bill,[*,§] and Shengfa Ye[*,†]

[†]Max-Planck-Institut für Kohlenforschung, Kaiser-Wilhelm-Platz 1, D-45470 Mülheim an der Ruhr, Germany
[§]Max-Planck-Institut für Chemische Energiekonversion, Stiftstr. 34-36, D-45470 Mülheim an der Ruhr, Germany

S *Supporting Information*

ABSTRACT: Iron(V)-nitrido and -oxo complexes have been proposed as key intermediates in a diverse array of chemical transformations. Herein we present a detailed electronic-structure analysis of $[Fe^V(N)(TPP)]$ (**1**, TPP^{2-} = tetraphenylporphyrinato), and $[Fe^V(N)(cyclam-ac)]^+$ (**2**, cyclam-ac = 1,4,8,11-tetraazacyclotetradecane-1-acetato) using electron paramagnetic resonance (EPR) and ^{57}Fe Mössbauer spectroscopy coupled with wave function based complete active-space self-consistent field (CASSCF) calculations. The findings were compared with all other well-characterized genuine iron(V)-nitrido and -oxo complexes, $[Fe^V(N)(MePy_2tacn)](PF_6)_2$ (**3**, $MePy_2tacn$ = methyl-N',N''-bis(2-picolyl)-1,4,7-triazacyclononane), $[Fe^V(N)\{PhB(t\text{-}BuIm)_3\}]^+$ (**4**, $PhB(^tBuIm)_3^-$ = phenyltris(3-*tert*-butylimidazol-2-ylidene)borate), and $[Fe^V(O)(TAML)]^-$ (**5**, $TAML^{4-}$ = tetraamido macrocyclic ligand). Our results revealed that complex **1** is an authenticated iron(V)-nitrido species and contrasts with its oxo congener, compound I, which contains a ferryl unit interacting with a porphyrin radical. More importantly, tetragonal iron(V)-nitrido and -oxo complexes **1−3** and **5** all possess an orbitally nearly doubly degenerate $S = 1/2$ ground state. Consequently, analogous near-axial EPR spectra with $g_{\parallel} < g_{\perp} \leq 2$ were measured for them, and their $g_{\parallel}$ and $g_{\perp}$ values were found to obey a simple relation of $g_{\perp}^2 + (2 - g_{\parallel})^2 = 4$. However, the bonding situation for trigonal iron(V)-nitrido complex **4** is completely different as evidenced by its distinct EPR spectrum with $g_{\parallel} < 2 < g_{\perp}$. Further in-depth analyses suggested that tetragonal low spin iron(V)-nitrido and -oxo complexes feature electronic structures akin to those found for complexes **1−3** and **5**. Therefore, the characteristic EPR signals determined for **1−3** and **5** can be used as a spectroscopic marker to identify such highly reactive intermediates in catalytic processes.
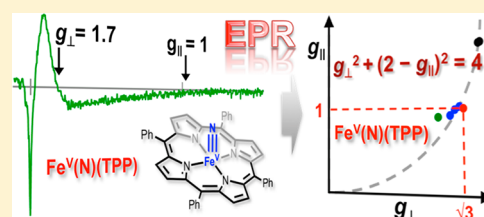
INTRODUCTION

High-valent iron complexes featuring oxo (O^{2-}) or nitrido (N^{3-}) coordination are invoked as key intermediates in O_2 and N_2 activation processes.[1] In biology, several nonheme iron(IV)-oxo intermediates have been trapped in the reactions of a series of O_2-activating iron enzymes, and were thoroughly characterized by absorption, resonance Raman (rR), and ^{57}Fe Mössbauer spectroscopy.[2] In parallel, synthetic chemists have prepared dozens of nonheme iron(IV)-oxo models in order to understand their structure−function relation.[3] Perferryl ($Fe^V = O$) complexes have also been proposed in the chemistry of nonheme iron enzymes.[4] Compound I, formally an iron(V)-oxo heme species, is pivotal intermediate of many heme-containing oxygenases and peroxidases (e.g., chloroperoxidase, horseradish peroxidase, and cytochrome P450 family),[5] which play crucial roles in a range of biological processes including mitochondrial respiration, steroid regulation and degradation of xenobiotics.[5b−e] However, ^{57}Fe Mössbauer measurements revealed that one of the oxidizing equivalents of compound I, in fact, is allocated to the porphyrin ligand, because its Mössbauer spectroscopic features are essentially identical to those of its one-electron reduced species, compound II

consisting of a triplet $Fe(IV) = O$ unit (Chart 1).[6] EPR investigations showed that the ferryl moiety and the porphyrin

Chart 1. Compound I and Compound II in Heme Containing Enzymes

Compound I   *Compound II*
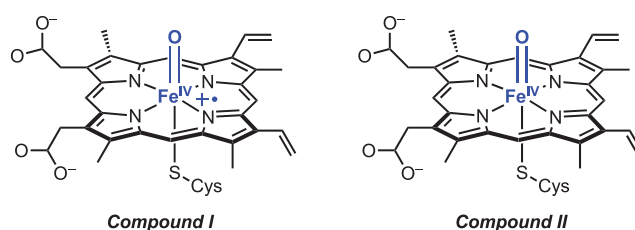
π radical of compound I are weakly antiferromagnetically coupled, thus yielding an overall doublet ground state ($S_{tot} = 1/2$).[7] However, model complexes of compound I all feature an $S_{tot} = 3/2$ ground state due to moderately strong ferromagnetic coupling.[8]

In contrast to a large number of iron-oxo compounds, only a few iron-nitrido complexes have been investigated to date,[9] despite the strong motivation to develop new nitrogen fixation protocols that may compete with the industrial Haber–Bosch process.[10] In 1988, Nakamoto and Wagner reported *in situ* generation and detection of the first iron(V)-nitrido species, $[Fe^V(N)(TPP)]$ (**1**, TPP^{2-} = tetraphenylporphyrinate dianion), a nitrido congener of compound I, using rR spectroscopy.[11] Complex **1** was generated by photo-oxidation of the corresponding iron(III)-azido precursor in the Raman laser beam. The rR spectra of **1** revealed the Fe–N stretching vibration at 876 cm^{-1} as well as several marker bands of the porphyrin ligand. Complex **1** was proposed to be a high spin ($S = 3/2$) iron(V)-nitrido compound without a ligand radical,[11b] by referring to its isoelectronic $[Mn^{IV}(O)(TPP)]$ complex.[12] This electronic structure assignment is qualitatively distinct not only from that determined for compound I, but also from those published later on for other well-characterized authenticated iron(V)-nitrido and -oxo complexes supported by innocent nonheme ligands, inasmuch as all possess low spin ($S = 1/2$) ground states (*vide infra*). Thus, the electronic structure of complex **1** needs to be further scrutinized by thorough spectroscopic investigations.

Recently, a handful of nonheme iron(V)-nitrido complexes (Chart 2), namely, $[Fe^V(N)(cyclam-ac)]^+$ (**2**, cyclam-ac =

Chart 2. Iron(V) Complexes Discussed in the Current Work
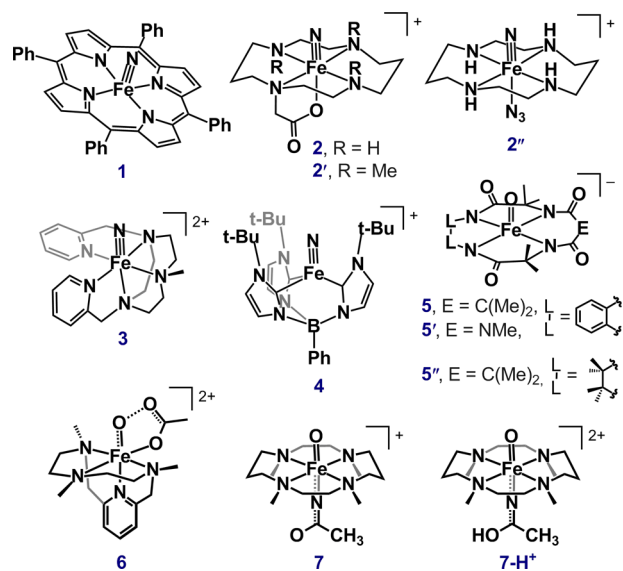
cyclam-1-acetato),[13] $[Fe^V(N)(Me_3\text{-cyclam-ac})]^+$ (**2′**, Me$_3$-cyclam-ac = 4,8,11-trimethylcyclam-1-acetato),[14] $[Fe^V(N)(N_3)(cyclam)]^+$ (**2″**),[15] and $[Fe^V(N)(MePy_2tacn)](PF_6)_2$ (**3**, MePy$_2$tacn = methyl-N',N''-bis(2-picolyl)-1,4,7-triazacyclononane),[16] were synthesized by bulk photolysis of their ferric-azido precursors in frozen solutions. Furthermore, complex $[Fe^V(N)L]^{2+}$ (L = 2,6-bis(1,1-di(aminomethyl)ethyl)pyridine) was produced in gas phase and detected by collision-induced dissociation of electrospray ionization mass spectrometry.[17] Complexes **2** and **3** have been characterized by ^{57}Fe Mössbauer and X-ray absorption spectroscopy coupled with DFT calculations.[13,14,16] It has been concluded that both complexes are best described as genuine low spin iron(V)-nitrido compounds. In addition to these tetragonal species, Smith, Meyer, and co-workers reported synthesis and spectroscopic

and structural characterization of a trigonal iron(V)-nitrido compound, $[Fe^V(N)(PhB(^tBuIm)_3)]^+$ (**4**, PhB(^{t}BuIm)$_3^-$ = phenyltris(3-*tert*-butylimidazol-2-ylidene borate). Complex **4** was also found to possess an $S = 1/2$ ground state despite featuring a different coordination geometry.[18]

Three bona fide iron(V)-oxo species have been reported thus far, $[Fe^V(O)(TAML)]^-$ (**5**, TAML^{4-} = tetraamido macrocyclic ligand),[19] and its biuretamide (**5′**) and beheaded (**5″**) derivatives.[20] EPR and ^{57}Fe Mössbauer measurements suggested that both complexes have a low spin ground state, in analogy to the nonheme iron(V)-nitrido complexes discussed above. Furthermore, iron(V)-oxo species have been advocated as actual oxidants for a range of nonheme iron complexes which catalyze regio- and stereoselective C—H and C=C bond functionalization.[21] Such iron(V)-oxo intermediates were generated by O—O bond cleavage of the corresponding metastable iron(III)-acetylperoxo precursors, $[Fe^{III}(OOAc)^-]^{2+}$. We recently carried out a detailed electronic structure analysis on $[Fe^V(O)(OAc)(PyNMe_3)]^{2+}$ (**6**, PyNMe$_3$ = 3,6,9,15-tetraazabicyclo[9.3.1]pentadeca-1(15),11,13-triene-3,6,9-trimethyl), an prototypical example of this type of catalysts. However, our results[22] showed that complex **6** is best formulated as an intermediate spin iron(IV) center antiferromagnetically coupled to an O—O σ* radical, viz. $[Fe^{IV}(O\cdots OAc)^{2-\bullet}]^{2+}$. As a result, **6** can be viewed as a three-electron reduced form of O$_2$ in which the O—O bond was not completely broken,[21b] as evidenced by a non-negligible negative spin population (−0.14) computed for the O atom in the acetate moiety, while the adjacent Fe^{IV}O unit featuring a large positive spin population (+1.17). A similar bonding situation was also encountered for $[Fe^V(O)(TMC)(NC(O)-CH_3)]^+$ (**7**, TMC = 1,4,8,11-tetramethyl-1,4,8,11-tetraazacyclotetradecane) and $[Fe^V(O)(TMC)(NC(OH)CH_3)]^{2+}$ (**7-H$^+$**).[23] Sizeable negative spin populations found on the N atoms of the *trans* ligands support the notion that complexes **7** and **7-H$^+$** contain a triplet ferryl unit that interacts with •N=C(O$^-$)CH$_3$ or •N=C(OH)CH$_3$ ligands in an antiferromagnetic fashion.[22]

Complex **1** cannot be generated by photolysis in fluid solution, because a mixed-valent iron(III/IV) μ-nitrido porphyrin dimer $[(TPP)Fe]_2N$ with an $S = 1/2$ ground state forms instead.[24] Similarly, complexes **2** and **3** also undergo facile decay by dimerization of the Fe^V=N groups, eventually yielding monomeric ferrous complexes and releasing N$_2$.[16,25] Because complexes **1**−**3** cannot persist in fluid solutions, their reactivity studies relied on *in situ* spectroscopic methods. For instance, complexes $[Fe^V(N)L]^{2+}$, **2** and **3** were shown to be capable of activating C—H or C=C bonds of organic substrates on the basis of the mass fragmentation analysis.[16,17,26] Nitride addition to CO and tri-*n*-butylphosphine for complexes **2** and **2″**, respectively, was monitored by time-resolved Fourier-transform infrared spectroscopy.[27] Furthermore, it was reported that treating complex **4**, the most stable iron(V)-nitrido compound, with cobaltocene and water leads to formation of ammonia.[18] Interestingly, in addition to initiating H- and O atom transfer processes,[28] complexes **5** and **5′** could act as cocatalysts for photochemical water oxidation.[29]

Although complexes **1**−**5** exhibit diverse chemical activity, detection of similar iron(V)-nitrido and -oxo intermediates in catalytic processes is rather challenging. Typically, ^{57}Fe Mössbauer and X-ray absorption spectroscopy are employed to identify such species. However, for both types of measurements there are some requirements for the sample

preparation and/or the availability of sophisticated facilities. More importantly, to reach unequivocal assignments of electronic structures, reference compounds, which are often homologous iron complexes with different oxidation states, are usually needed. Because of these limitations, alternative spectroscopic technique that allows to detect transient iron(V)-nitrido and -oxo complexes with higher efficiency and higher sensitivity is highly desirable.

The present work serves as a dual purpose. We first present a combined spectroscopic and computational study of the electronic structure of complex **1** in comparison with well-characterized iron(V) complexes **2**−**5**. This enables us to identify the unique bonding feature of tetragonal low spin iron(V)-nitrido and -oxo complexes. On the basis of that, we propose characteristic EPR signatures for such species. Note that correlation of the electronic structure of trigonal iron(V)-nitrido complex **4** with its g factors was published earlier by Smith, Kirk and Hoffman and co-workers.[30]

■ MATERIALS AND METHODS

Sample Preparation and Photolysis. The ferric azido complexes, $[Fe^{III}(N_3)(TPP)]$ (**1**[pro])[31] and $[Fe^{III}(N_3)(cyclam-ac)]$-$(PF_6)$ (**2**[pro]),[13a] were synthesized by following the published procedures. Dry and degassed solvents were used to prepare the samples. The ferric azido precursors were dissolved in a 1:9 dichloromethane:toluene mixture for **1**[pro] or 1:9 methanol:*n*-butyronitrile for **2**[pro] to give 2 mM stock solutions. Aliquots of the azide solutions were loaded into standard 4 mm quartz EPR tubes before freezing in liquid nitrogen. Then, the tubes were placed in a finger Dewar filled with liquid nitrogen and photolyzed by an LED LUXEON III Star LED lamp (dominant wavelength of 470 nm). The entire photolysis to generate complex **2** in the EPR tubes was completed within 30 min, whereas for complex **1**, the irradiation had to last for ca. 20 h. To prepare Mössbauer samples, droplets of the frozen solution of fully ^{57}Fe-enriched **1**[pro] (1.7 mM in the solvent mixture) were collected in liquid nitrogen and crushed into fine powder, which was then photolyzed for 18 h accompanied by periodic manual stirring. The powder was subsequently recovered from liquid nitrogen slurry and transferred to Mössbauer sample cups (ca. 0.7 mL). The photolyzed samples were always stored in liquid nitrogen to avoid decomposition of the desired iron(V)-nitrido species. An EPR sample of photolyzed **1**[pro] was subjected to rR measurements to validate the formation of **1**.

EPR Measurements. Continuous-wave (cw) X-band EPR measurements were performed on a Bruker E500 ELEXSYS spectrometer equipped with the Bruker dual-mode cavity (ER4116DM) or a standard cavity (ER4102ST) and an Oxford Instruments helium flow cryostat (ESR 900). The microwave bridge was a high-sensitivity Super-X bridge (Bruker ER-049X) with integrated microwave frequency counter. The magnetic field controller (ER032T) was calibrated with a Bruker NMR field probe (ER035M). EPR simulations have been done with our own routines, esim_gfit and esim_sx. For spin quantitation, the experimental derivative spectra were numerically integrated by using the routine eview, and the results were corrected for their g value dependence for field-swept spectra by using Aasa and Vänngård approximation,[32] i.e. dividing the integrals by the factor,

$$g_P^{av} = \frac{2}{3}\sqrt{\frac{\sum_i g_i^2}{3}} + \frac{\sum_i g_i}{9}$$

^{57}Fe Mössbauer Measurements. ^{57}Fe Mössbauer spectra were recorded on a conventional spectrometer with alternating constant acceleration of the γ-source (^{57}Co/Rh, 1.8 GBq), which was kept at room temperature. The minimum experimental line width was 0.24 mm/s (full width at half-height). The sample temperature was maintained constant in an Oxford Instruments Variox cryostat. Isomer shifts are quoted relative to iron metal at 300 K.

Computational Setup. All calculations were performed by using the ORCA quantum chemical program.[33] For geometry optimizations, the BP86[34] functional was used in combination with the resolution of the identity (RI)[35] approximation. All atoms were described by the triple-ζ quality def2-TZVP basis set in conjunction with the def2-TZV/J auxiliary basis set required for the RI approximation.[36] Solvation effects were taken into account by employing the conductor like polarizable continuum model (CPCM),[37] for which, to be consistent with the experiment, acetonitrile (ε = 36.6) was chosen as the solvent. Numerical frequency calculations verified the optimized structures to be local minima on the potential energy surface.

The complete active space self-consistent field (CASSCF) calculations[38] were performed with the def2-TZVPP basis set along with the def2-TZVPP/C auxiliary basis set for the RI approximation. In the case of complexes **1**−**3** and **5**, we first tested CASSCF(11,9) calculations, for which the active space consists of five d-orbitals, three nitrido- or oxo-2p based orbitals, respectively, and the bonding combination (σ_{eq}) with respect to the interaction between the Fe $d_{x^2-y^2}$ orbital and the equatorial ligands. It turned out that the CASSCF(11,9) computations predicted an erroneous ground state with an electron configuration of $(nb)^2(\sigma*_{eq})^1$ instead of $(nb)^2(\pi*_{Fe-N})^1$. As a consequence, the computed g-values deviate from the experiment values significantly. We then enlarged the active space by adding three t_{2g}-derived 4d orbitals ($4d_{xy}$, $4d_{xz}$, and $4d_{yz}$), and the resulting CASSCF(11,12) computations provided a correct ground state as evidenced by the calculated g-values closely matching the experiment. For complex **1**, in order to allow development of radical character in the porphyrin ligand, we also added four porphyrin π-orbitals, namely, a_{1u}, a_{2u}, and two e_g orbitals on top of CASSCF(11,12). The resulting CASSCF(15,16) calculations with an active space containing more than 14 orbitals were treated by iterative-configuration expansion configuration interaction (ICE-CI), an approximated version of the full configuration interaction recently developed by our group. For complex **4**, we employed an active space distributed 13 electrons into 14 orbitals CASSCF(13,14), including five Fe d-orbitals, three nitrido 2p based orbitals, two bonding partners of the d_{xy} and $d_{x^2-y^2}$ orbitals, and four 4d orbitals ($4d_{xy}$, $4d_{x^2-y^2}$, $4d_{xz}$ and $4d_{yz}$). To capture dynamic correlation effects, N-electron valence perturbation theory of second order (NEVPT2)[39] calculations were performed on top of the CASSCF wave functions.

For g-value calculations using the multireference CASSCF/NEVPT2 method,[40] we first diagonalized the spin−orbit coupling (SOC) matrix constructed by the five roots from the state-average CASSCF calculation, for which the diagonal elements were replaced by the NEVPT2 excitation energies. The g-values were then computed by using Gerloch−McMeeking equation in the basis of the relativistic wave functions, the eigenvectors of the SOC matrix.[41]

■ RESULTS AND DISCUSSION

Spectroscopic Characterizations of Iron(V)-Nitrido Species. In the earlier work, the electronic structure of complex **1** was deduced only from its vibrational frequencies determined by the rR measurements.[11] In order to gain more insights into its nature, we carried out more thorough spectroscopic characterizations. In the present work, complex **1** was prepared by irradiating frozen solutions of **1**[pro] in quartz EPR tubes for 20 h. The samples thus obtained are closer to the usual conditions of chemical reactions in comparison with the previous work, where complex **1** was generated by photolysis of a solid thin film of **1**[pro] deposited on a cold tip in the incident Raman beam at 30 K.[11] Despite the different preparation protocol employed, the rR spectra measured for our photolyzed samples revealed signals at 883, 1371, and 1569 cm^{-1} (Figure S5), which reasonably match the Fe—N stretching vibration and the marker bands of the porphyrin ligand reported before for **1** (876, 1373, 1576 cm^{-1},

respectively).[11b] The difference can be attributed to the solvent effect. Thus, the rR investigations confirmed the successful generation of complex **1**.

The zero-field Mössbauer spectrum (Figure 1) of the photolyzed sample, which is prepared in a similar way by
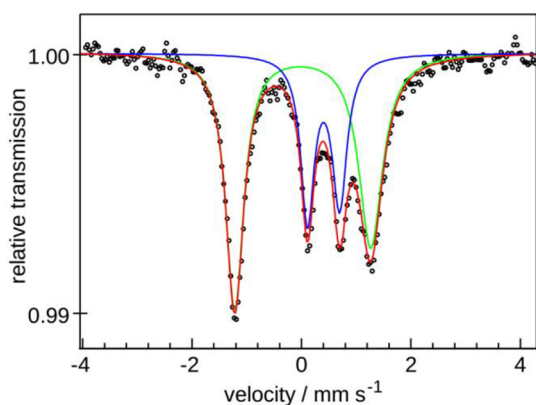

Figure 1. Mössbauer spectrum of 18 h-photolyzed **1**^{pro} measured at 80 K. The simulation (red line) is composed of two components. Parameters: δ = 0.02, $|\Delta E_Q|$ = 2.49, Γ = 0.40 mm/s, $w_{2/1}$ = 1.32 (67%, green line), and δ = 0.40, $|\Delta E_Q|$ = 0.59, Γ = 0.30 mm/s, $w_{2/1}$ = 1.10 (33%, blue line). Γ is the full-width at half-maximum of the Lorentzian lines and $w_{2/1}$ is the asymmetric broadening factor for the high-energy line of the doublets. The asymmetric broadening is introduced to mimics the effects of not perfectly fast spin relaxation for a half-integer spin species.

starting from ^{57}Fe-enriched **1**^{pro}, exhibits two quadrupole doublets. The minor component can be attributed to the unreacted precursor as compared to the Mössbauer spectrum independently measured for **1**^{pro} (Figure S6). The newly formed major component that is assigned to **1** accounting for 67% of the total iron content in the sample has an isomer shift of 0.02 mm/s and a quadruple splitting of 2.49 mm/s. Notably, the isomer shift of **1** is comparable to those found for complexes **2**, **2'**, **2''**, and **3** (Table 1), indicating that the iron oxidation states of **1** is also +V. The more negative isomer shifts observed for complexes **4**, **5**, **5'**, and **5''** mainly originate from the more contracted Fe—N/O bonds. Typically, the iron-ligand distance is a more critical factor than the d^N configuration of the iron center to determine the isomer shift, i.e. the shorter the iron-ligand distance, the more negative the isomer shift.[42] Consequently, to reach more reliable conclusion about the iron oxidation state, it is necessary to compare the isomer shifts of related complexes with similar chemical bonding.

Complex **1**^{pro} produces a nearly axial EPR spectrum with effective g factors of 6.02, 5.89, and 2.01 (Figure 2, traces a),
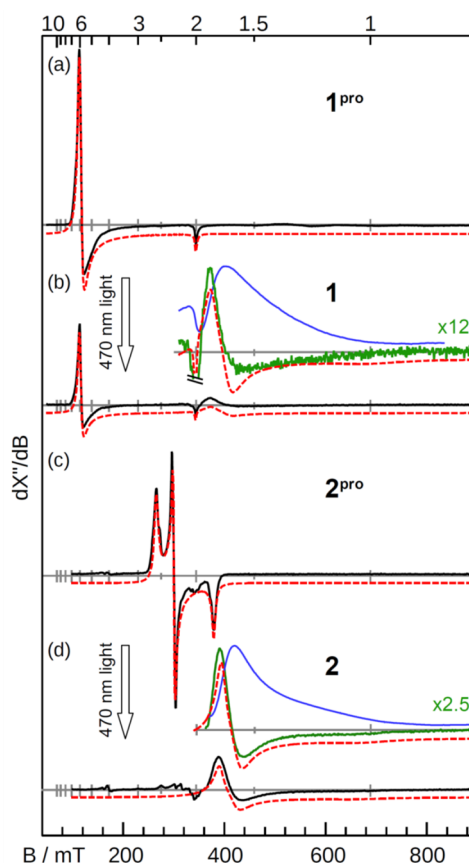

Figure 2. X-Band EPR spectra of **1** and **2** in situ prepared from the azide precursors. Spectra a and c are **1**^{pro} and **2**^{pro}; spectra b and d were obtained after photolysis of **1**^{pro} (a) and **2**^{pro} (c) (black traces). The insets show amplified signals (green traces) and their integrated absorption spectra (blue lines) at higher field region. Simulations are shown in red dashed lines. Conditions: 10 K with 0.2 nW microwave power and 0.75 mT modulation amplitude.

typical for high spin iron(III) porphyrin complexes (S = 5/2) with a positive axial zero-field splitting. After 20 h of photolysis, the signal of **1**^{pro} is attenuated, and a weak yet perceptible asymmetric zero-crossing signal around 400 mT appears with a very shallow trough extending to the high field (Figure 2, traces b), rendering an almost axial spectrum with $g_{\parallel}$ < $g_{\perp}$ ≤ 2. The resonances are attributed to complex **1**. A reasonable fit gave g factors of 1.83, 1.70, and 1.0 for **1**,

Table 1. Spectroscopic Parameters of Iron(V) Complexes

Fe^V complex	Fe—N/O distance (Å)	δ (mm s^{-1})	$|\Delta E_Q|$ (mm s^{-1})	g-values[a]	ref.
1		0.02	2.49	1.83, 1.70, 1.0 (1.766, 1.718, 0.931)	this work
2	1.61	−0.04	1.67	1.75, 1.64, 1.0[b] (1.542, 1.510, 0.512)	13a
2'				1.68, 1.55, 0.92	14
2''		−0.04	1.90	1.75, 1.63, 0.99	14, 15
3	1.64	−0.01	1.02	1.59, 1.33, 0.9 (0.974, 0.962, 0.041)	16
4	1.506(2)	−0.45[c]	4.78[c]	2.299, 1.971, 1.971 (2.275, 1.990, 1.981)	18
5	1.58	−0.42	4.25	1.99, 1.97, 1.74 (2.033, 1.947, 1.803)	19
5'		−0.44	4.27	1.983, 1.935, 1.726	20a
5''		−0.42	4.25	2.02, 1.98, 1.84	20b

[a]In parentheses are the g-values calculated at the CASSCF/NEVPT2 level. [b]EPR data obtained in this work. [c]Values recorded at 78 K.

wherein g_{min} was estimated on the basis of the integrated absorption spectrum and fixed in the simulation. Double integration of the spectra, for which the g-dependence of the field-swept spectra was adjusted by Aasa-Vænngård factors,[32] revealed that the yield of the 1^{pro}-to-1 conversion is 71% (Figures S3 and S4), comparable to that determined by the Mössbauer measurements. This observation hence confirms our assignment of the emerged EPR signal to 1.

For comparison, photolysis of 2^{pro} was carried out at the same conditions. Unlike that of 1^{pro}, the photoreaction of 2^{pro} in the EPR tubes completed within half an hour. Low spin ferric azido complex 2^{pro} elicits a rhombic spectrum with large g-anisotropy[13a] (Figure 2, traces c, g_{max} = 2.60, g_{mid} = 2.29, and g_{min} = 1.82). After photolysis, it completely changed into a wide-split spectrum at low g values that we attributed to the photolysis product, 2 (Figure 2, traces d). The simulations yield g factors of 1.75, 1.64, and 1.0 for 2, similar to those detected for 1. Double integration of the spectra demonstrated nearly full recovery of the spin in the conversion of 2^{pro} to 2. Remarkably, such unconventional EPR spectra with three g factors all significantly lower than 2 were also observed for complexes $2'$, $2''$,[14] and 3^{16a} (Table 1).

Taken together, complex 1 must feature qualitatively the same electronic structure as those determined for 2 and 3. This notion is consistent with the observation that the Fe—N stretching frequency measured for 1 (883 cm^{-1}) is comparable to those for 2 (864 cm^{-1})[13c] and 3 (866 cm^{-1}).[16b] Therefore, complex 1 is a genuine iron(V)-nitrido species and possesses a low spin rather than high spin ground state. Different from complexes 2 and 3 whose precursors are both low spin complexes, 1 is evolved from a high spin complex. Thus, the formation of 1 must involve a change in the spin state. Our B3LYP calculations predicted the quartet state to be ~15 kcal/mol higher in energy than the doublet ground state. One can anticipate an even large gap for the sextet state in which all iron-nitrido antibonding orbitals are singly occupied. As such, the large driving force and the efficient spin-orbit coupling (SOC) of the iron center may render the required spin transition easily occur. Clearly, our findings show that low spin state of the ferric azido precursors is not the prerequisite for the photochemical generation of iron(V)-nitrido species.[43]

The EPR spectrum of 1 differs markedly from those of the various forms of compound I, whose S_{tot} = 1/2 ground state results from (weak) antiferromagnetic coupling between a triplet ferryl core and a porphyrin π-radical.[7] Because the isotropic exchange coupling (J) competes with the axial zero-field splitting of the ferryl moiety ($D_{Fe=O}$), the nature of the ground state depends on the degree of the resulting mixing of S_{tot} = 1/2 and 3/2. As a consequence, the EPR spectra of the variants of compound I in different enzymes vary depending on the relative magnitudes of J and $D_{Fe=O}$. For instance, g factors below 2 have been observed for compound I in chloroperox-idase[6c] ($g_{\parallel}$ = 2 and broad $g_{\perp} \approx 1.73$, $J/D \approx 1$), and the EPR spectrum of horseradish peroxidase shows an exceedingly broad feature at $g \approx 1.99$ due to a much smaller $J/D_{Fe=O}$ value and conformational strains.[7a] In general, the spin Hamiltonian analyses[7a,c] render the sharp $g_{\parallel}$ feature close to 2 nearly independent of the $J/D_{Fe=O}$ value, whereas $g_{\perp}$ can be much smaller. Interestingly, the synthetic porphyrin model complexes of compound I show distinct S_{tot} = 3/2 ground states with effective g values of $g_{\perp}^{eff} \approx 4$ and $g_{\parallel}^{eff}$ = 2, independent of various porphyrin substitutions.[8] The situation for compound I and its models is thus distinct from that observed for 1, which

features $g_{\parallel} < g_{\perp} \leq 2$. This finding further corroborates that complex 1 and compound I possess different electronic structures.

The EPR spectrum of complex 5 displays a near-axial pattern of $g_{\parallel} < g_{\perp} \leq 2$,[19] similar to that found for complexes $1-3$, but has much smaller g shifts, the deviation of the measured g value from spin-only g value, 2. In contrast, a distinct EPR spectrum with $g_{\parallel} < 2 < g_{\perp}$ is observed for complex 4.[18] These observations hence give rise to a question about how to correlate the different g factors determined for complexes $1-5$ with their electronic structures.

Ligand Field Analysis of Electronic Structures of Iron(V)-Nitrido/-Oxo Complexes and Their g Values. In this section, we first present a ligand-field bonding analysis of iron(V)-nitrido and -oxo complexes in tetragonal and trigonal coordination environments. On the basis of that, a quantitative model to rationalize the g values of tetragonal low spin iron(V)-nitrido and−oxo complexes ($1-3$ and 5) is developed. In the next two sections, the approximation used to derive this model will be verified by more rigorous multireference electronic-structure calculations using the CASSCF/NEVPT2 approach and finally the validity of the model will be carefully evaluated.

As elaborated elsewhere[44] the interaction of the iron center with oxo and nitrido ligands (E) is rather covalent and entails two π-bonds between the Fe-$d_{xz/yz}$ and E-$p_{x/y}$ orbitals, and one σ-bond involving the Fe-d_{z^2} and E-p_z orbitals. The resulting antibonding molecular orbitals are labeled as π^*_{Fe-E} with a 2-fold degeneracy and σ^*_{Fe-E}, respectively. For tetragonal coordination geometry, the remaining d_{xy} orbital is essentially a nonbonding (nb) orbital, whereas $d_{x^2-y^2}$ interacts strongly with the equatorial donors of the supporting ligand, yielding the σ^*_{eq} molecular orbital. Thus, one envisions a 1+2+1+1 ligand field splitting pattern (Scheme 1a) with the energetic

Scheme 1. Qualitative Orbital Splitting Pattern for Iron(V) Complexes
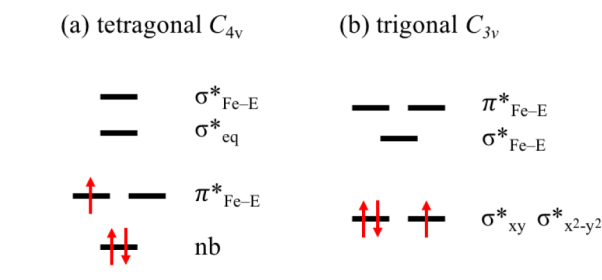
ordering of nb < π^*_{Fe-E} < σ^*_{eq} (the σ^*-orbital in the equatorial plane) < σ^*_{Fe-E}, as proposed for complex $[V^{IV}(O)(H_2O)_5]^{2+}$ by Ballhausen and Gray.[45] For low spin d^3 centers, the only unpaired electron must occupy one of the doubly degenerate π^* orbitals, and the resulting electron configuration of $(nb)^2(\pi^*)^1$ leads to a ground state of ^2E symmetry in the C_{4v} point group. However, even in ideal cases where the supporting ligands possess 4-fold rotation axes, such as TPP, Jahn−Teller distortions should lower the symmetry of the entire complex and lift the double degeneracy of the ^2E state.

In the case of trigonal coordination geometry, a 2+1+2 ligand field splitting with the energetic ordering of $2\sigma^*_{eq}$ < $\sigma^*_{Fe-E} \leq 2\pi^*_{Fe-E}$ (Scheme 1b) is often proposed, where σ^*_{eq} is the equatorial σ^*-combination between the d_{xy} and $d_{x^2-y^2}$

orbitals and the equatorial donors of tripodal ligands. Note that the equatorial σ-antibonding interaction in pseudotetrahedral geometry is much weaker than the corresponding one in distorted octahedral or square pyramidal coordination arrangements. In the latter cases, the four lobes of the $d_{x^2-y^2}$ orbital all directly point to the donor atoms. Therefore, in a trigonal coordination environment the σ^*_{eq} orbitals usually have the lowest energy. Because of the $3d_{z^2}$-$4s$-$4p_z$ mixing, σ^*_{Fe-E} is typically situated at lower energy than π^*_{Fe-E}.[9b] Note that for a trigonal iron(IV)-nitrido complex supported by a bulky guanidinate ligand, DFT calculations suggest that the π^*_{Fe-N} orbitals lie above σ^*_{Fe-N}.[46] Despite this complexity, for low spin iron(V) complexes, the singly occupied molecular orbital (SOMO) must be one of the two σ^*_{eq}-orbitals. Consequently, the ground state is predicted to feature a $(\sigma^*_{xy,\ x^2-y^2})^3$ electron configuration, and to be of ^2E symmetry in the C_{3v} point group. Similar to the tetragonal situation discussed above, even when the supporting ligands possess three-fold rotation axes, the double degeneracy of ^2E cannot be maintained.

To gain further insight into the correlation between the electronic structure and the EPR g values of low spin iron(V) complexes, one needs to consider SOC between the ground state and low lying excited states with the same spin as the ground state. The g anisotropy and g shifts are predominantly originated from the mixing of excited states into the ground state under the influence of SOC and the resulting partial restoration of the orbital angular moment.[47] The sign of the g shifts can be predicted by using the following rule.[47] A DOMO-to-SOMO (DOMO = doubly occupied molecular orbital) transition causes a positive g shift, whereas a SOMO-to-VMO (VMO = virtual molecular orbital) transition gives a negative g shift. The magnitude of the g shift is inversely proportional to the excitation energy.

As will be verified below, due to the overwhelming iron-nitrido and −oxo interaction, complexes **1−3** and **5** feature an orbitally near doubly degenerate ground state. More importantly, the energy separation between the ground state with an electron configuration of $(nb)^2(\pi^*_y)^1$ and the first excited state $(nb)^2(\pi^*_x)^1$ is comparable to the effective SOC constant of iron(V) ($\sim$578 cm^{-1}).[48] Thus, we assume that the SOC within the effective ^2E ground state essentially dictates the g values, and the contributions from the higher lying excited states are negligible. According to the above rule, for **1−3**, **5**, the lowest-energy SOMO-to-VMO excitation $(nb)^2(\pi^*_y)^1 \rightarrow (nb)^2(\pi^*_x)^1$ should give a dominant down-shift of one g value ($g_{\parallel}$), as experimentally measured, whereas for trigonal complex **4**, the lowest-energy DOMO-to-SOMO excitation of $\sigma^*_{xy} \rightarrow \sigma^*_{x^2-y^2}$ should introduce a positive g shift in the z direction along the Fe—N bond. The (smaller) negative shift found for $g_{\perp}$ is in accord with the two higher lying SOMO-to-VMO excitations of $\sigma^*_{x^2-y^2} \rightarrow \pi^*_{x/y}$.

In order to rationalize more quantitatively the g values of **1−3** and **5**, which largely determined by the intra-^2E excitations $((nb)^2(\pi^*_y)^1 \rightarrow (nb)^2(\pi^*_x)^1)$, we first consider an ideal situation where complexes have an exact doubly degenerate ^2E ground state. In this case, one can show that only the $\hat{l}_z \cdot \hat{s}_z$ term contributes nonvanishing matrix elements to the SOC Hamiltonian (For details, see the Supporting Information), which, hence, can be written as

$$\hat{H}_{SOC} = \zeta \hat{l}_z \cdot \hat{s}_z$$

Here to a good approximation the SOC operator is treated as a single-electron operator.[47a]

Furthermore, to simplify the calculation, one can use complex d-orbitals, which are eigenfunctions of $\hat{l}_z$. These complex d-orbitals are related to the usual real d-orbitals by a unitary transformation. Specifically, the two degenerate real d_{xz} and d_{yz} orbitals in C_{4v} symmetry correspond to the complex d_{+1} and d_{-1} orbitals. Thus, the four basis functions of the ^2E state can be characterized by the orbital and spin magnetic quantum numbers, L_M and S_M, viz. $|L_M S_M\rangle$.

Specifically,

$$\left|+1+\frac{1}{2}\right\rangle = |\alpha_{Fe}d^{\alpha}_{+1} + \alpha_N p^{\alpha}_{+1}\rangle, \quad E \approx +\frac{1}{2}\alpha^2_{Fe}\zeta_{Fe}$$

$$\left|-1-\frac{1}{2}\right\rangle = |\alpha_{Fe}d^{\beta}_{-1} + \alpha_N p^{\beta}_{-1}\rangle, \quad E \approx +\frac{1}{2}\alpha^2_{Fe}\zeta_{Fe}$$

$$\left|+1-\frac{1}{2}\right\rangle = |\alpha_{Fe}d^{\beta}_{+1} + \alpha_N p^{\beta}_{+1}\rangle, \quad E \approx -\frac{1}{2}\alpha^2_{Fe}\zeta_{Fe}$$

$$\left|-1+\frac{1}{2}\right\rangle = |\alpha_{Fe}d^{\alpha}_{-1} + \alpha_N p^{\alpha}_{-1}\rangle, \quad E \approx -\frac{1}{2}\alpha^2_{Fe}\zeta_{Fe}$$

Here the coefficients α_{Fe} and α_N denote the contributions from iron 3d- and nitrido or oxo p-orbitals, and the indices α and β at the d and p functions denote the spin part. Apparently, $|L_M S_M\rangle$ is the eigenfunction of the SOC operator, and its energy E is obtained by acting the SOC Hamiltonian on itself. Furthermore, ζ_{Fe} is the effective SOC constant of Fe(V), whereas the SOC of the ligand-atoms is neglected. In summary, as expected, the ^2E ground state in perfect C_{4v} symmetry is split by the first-order SOC into two Kramers doublets.

Lowering the symmetry from C_{4v} to the actual symmetry C_1 of the complexes under investigation leads to mixing of $|+1S_M\rangle$ and $|-1S_M\rangle$, because eventually only S_M is a good quantum number. Such mixing can be parametrized in terms of a mixing angle φ ($\varphi \in [0, \pi/4]$), which yields the wave functions of the lowest-energy Kramers doublet as

$$|\alpha\rangle = \sin\varphi\left|+1+\frac{1}{2}\right\rangle + \cos\varphi\left|-1+\frac{1}{2}\right\rangle$$

$$|\beta\rangle = \sin\varphi\left|-1-\frac{1}{2}\right\rangle + \cos\varphi\left|+1-\frac{1}{2}\right\rangle$$

Furthermore, the Zeeman splitting is described by

$$\hat{H}_Z = \mu_B(\hat{l} + g_e\hat{s})\vec{B}$$

Here μ_B is the Bohr magneton, $g_e \approx 2$ is the spin-only g value, and B is the magnetic field. For a given isolated doublet, one can compute the g values as defined for Kramers doublets in a weak-field approximation by using

$$g = \frac{\Delta E}{\mu_B B}$$

To this end, the Zeeman matrix for the magnetic field along the Z direction can be computed as follows

$$\begin{pmatrix} +2\sin^2\varphi & 0 \\ 0 & -2\sin^2\varphi \end{pmatrix}\mu_B B$$

Therefore,

$$\Delta E = 4\mu_B B \sin^2 \varphi$$

$$g_\parallel = 4\sin^2 \varphi \qquad (1)$$

Similarly, for the magnetic field in the equatorial plane, the Zeeman matrix is

$$\begin{pmatrix} 0 & \sin 2\varphi \\ \sin 2\varphi & 0 \end{pmatrix} \mu_B B$$

and

$$g_\perp = 2|\sin 2\varphi| \qquad (2)$$

Note that the final g matrix computed by this approach is only determined by the mixing angle φ and is independent of the metal−ligand covalency parametrized by α values (for details, see the Supporting Information).

One can eliminate φ in eqs 1 and 2, and obtain a direct relation between the two g factors.

$$g_\perp^2 + (2 - g_\parallel)^2 = 4 \qquad (3)$$

This equation represents the lower quadrant of a full cycle with a radius of 2 and the origin at (0,2) (Figure 3). In the
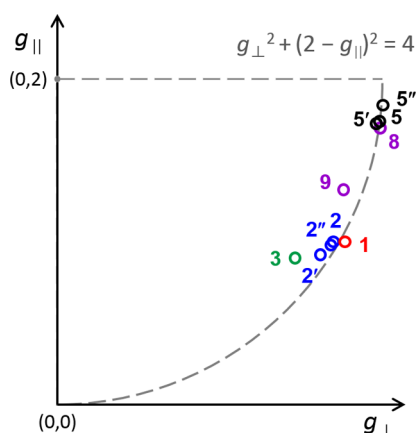

Figure 3. Schematic relationship of g factors of tetragonal Fe^V complexes. The $g_\perp$ is the average of the two slightly different g values of each compound.

present case, if the energy gap between the two components of ^2E is zero, then $g_\parallel = g_\perp = 0$. Because the two components of the lowest energy Kramers doublet have orbital angular momenta of $\pm\hbar$ and spin angular momenta of $\mp\hbar/2$, the magnetic moment arising from the orbital angular momentum exactly cancel out that from the spin angular momentum. However, if the energy separation is close to infinity, then $g_\parallel = g_\perp = 2$, because the orbital angular momentum is completely quenched and the system has an orbitally nondegenerate ground state. The g values determined experimentally for complexes **1−3** and **5** all obey eq 3 nicely.

Ab Initio Calculations of Electronic Structures of Iron(V)-Nitrido-/-Oxo Complexes. As analyzed above, to rationalize g values of transition metal complexes, one need to consider the SOC between the ground state and low lying excited states, especially for complexes **1−5** which likely feature orbital near degeneracy. In this regard, DFT is not a method of choice, because it cannot treat the ground and excited states on an equal footing.[49] Therefore, it is necessary

to employ wave function based highly correlated CASSCF/NEVPT2 approach. In our earlier work on the spectroscopy and reactivity of high valent iron-oxo complexes,[22,50] this method has been shown to deliver reliable results not only for the ground state but also for the excited states. The balanced active space should consist of the Fe-centered 3d orbitals and their ligand centered bonding partners. For complexes **1−3**, the active space has to include three t$_{2g}$ derived 4d orbitals ($4d_{xy}$, $4d_{xz}$, and $4d_{yz}$); otherwise, the CASSCF calculations predicted erroneous ground states (for details, see the Supporting Information). To examine the electronic structure of complex **1** in an unbiased manner, we further added four porphyrin π-orbitals, namely, a$_{1u}$, a$_{2u}$, and two e$_g$, into the active space, which should allow the system to develop a porphyrin radical in the calculations. Hereafter, we first discuss the ground state of complexes **1−5**, and then discuss their excited states.

As displayed in Figure 4, our CASSCF(15,16) calculations on complex **1** revealed that its ground state features a principal electron configuration (74%) of (nb d_{xy})^2(σ_{eq})^2(σ_z)^2 ($\pi_{x/y}$)^4(a$_{1u}$)^2(a$_{2u}$)^2(π^*_y)^1(π^*_x)^0(e$_{g\text{-}x/y}$)^0(σ^*_{eq})^0(σ^*_z)^0. Thus, our theoretical results reinforced that complex **1** cannot be

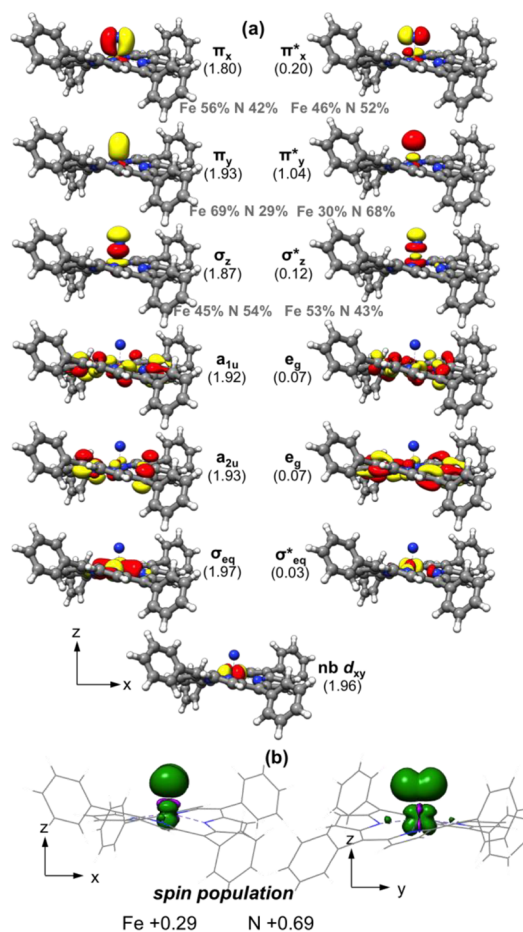**Figure 4.** Electronic structure of complex **1**. (a) Natural orbitals obtained from the ground-state CASSCF(15,16) calculation. The occupation number of each orbital is shown below the orbital label (nb = nonbonding) and atomic contributions to the molecular orbitals are shown for the important orbitals. The double d-shell is omitted for clarity. (b) Spin density and population obtained at the CASSCF(15,16) level.

formulated as an iron(IV)-nitrido species interacting with a porphyrin radical. The same bonding picture was delivered by the CASSCF(11,12) calculations (Figure S13); therefore, in the following we employed the smaller active space to compute its low lying ligand-field excited states. The predicted ground-state electron configuration of complex **1** corresponds to one component of the ^2E state. To accommodate such a ground state for complex **1**, the optimized geometry shows that the Fe center is situated above the porphyrin plane, and that the two Fe−N bonds (1.981, 1.974 Å) along the *x*-direction are considerably shorter than those (2.000, 1.996 Å) along the *y*-direction (Figure S19). These geometric distortions raise the π^*_x orbital and simultaneously lower the π^*_y orbital.

Unexpectedly, the computed spin population of the iron center in complex **1** is less than that of the nitrido ligand. In line with this observation, the $\pi^*_{x,y}$ orbitals contains more N-$p_{x,y}$ contribution than that from the Fe-$d_{xz,yz}$ atomic orbitals. Thus, the iron-nitrido interaction features so-called "inverted" bonding,[44c,51] in contrast to usual situations where the metal d character prevails in metal−ligand antibonding orbitals. Thus, there is substantial radical character in the nitrido ligand of complex **1**, and its electronic structure is best described as a resonance hybrid between two limiting bonding situations, $Fe^V(S_{Fe} = 1/2)N^{3-} \leftrightarrow Fe^{II}(S_{Fe} = 0)N^{\bullet}(S_N = 1/2)$, in the latter case the iron center featuring an electron configuration of $(d_{xy})^2(d_{xz})^2(d_{yz})^2$. This bonding description is consistent with that deduced from the earlier ground-state DFT calculations.[13b] However, for iron(V)-oxo complex **5**, the spin population of the iron center is higher than that of the oxo group (Figure S17). The difference clearly originates from considerably higher energy of the nitrido p-orbitals than the oxo p-orbitals. Furthermore, as analyzed in our earlier work on related iron(IV)-oxo complexes,[22,50] the unpaired electron in the SOMO (π^*_y) is expected to contribute positive spin density in the Fe-d_{yz} and N-p_y atomic orbitals, while negative spin density on the iron center, which reduces the total spin population, mainly stems from the spin polarization. Because in the present case, the nitrido ligand has a larger spin population than the iron center, spin polarization induces some marginal negative spin density in the Fe-d_{xz} and -d_{z^2} atomic orbitals as suggested by the occupation numbers of the DOMOs (π_x and σ_z) substantially deviating from their anticipated value (2), and those of the corresponding VMOs (π^*_x and σ^*_z) considerably differing from 0. Consequently, the spin density does not exactly resemble the shape of the SOMO and shows a negative fraction in the *xz* plane (Figure 4b). The situation found for complex **1** is exclusively different from those for **6**, **7**, and **7-H⁺** where the peripheral groups of the central Fe^{IV}O unit possess sizable negative spin density.[22]

Relative to **1**, similar leading electron configurations were found for the ground states of complexes **2**, **3**, and **5** (Figures S14, S15, and S17). For complex **2**, the double degeneracy of the effective ^2E ground state is lifted by the interaction of the iron center with the *trans* π-donating acetate ligand. The optimized geometries of complexes **3** and **5** reveals that the iron centers move out of the equatorial plane and that the computed equatorial metal−ligand bond distances along the *x*-direction substantially differ from those along the *y*-direction (Figure S19), an analogous situation found for complex **1**. Such geometric distortions stabilize one of the two components of the ^2E ground states, and destabilize the other.

Table 2 summarizes the calculated energies of important excited states for all complexes under investigation. Complexes

Table 2. CASSCF/NEVPT2 Excitation Energy (cm⁻¹) for Complexes 1−5

Excitation	$\pi^*_y \rightarrow \pi^*_x$	$\pi^*_y \rightarrow \sigma^*_{eq}$	$nb \rightarrow \pi^*_y$	$\pi^*_y \rightarrow \sigma^*_z$
Excited state	$(nb)^2(\pi^*_x)^1$	$(nb)^2(\sigma^*_{eq})^1$	$(nb)^1(\pi^*_y)^2$	$(nb)^2(\sigma^*_z)^1$
1	630	3870	22950	13260
2	400	4890	20770	20480
2′	500	2790	20180	20580
2″	450	5710	20160	20010
3	130	5020	20880	20580
5	2470	29370	13630	14610
5′	2380	28910	14440	14800

Excitation	$\sigma^*_{xy} \rightarrow \sigma^*_{x^2-y^2}$	$\sigma^*_{x^2-y^2} \rightarrow \pi^*_x$	$\sigma^*_{x^2-y^2} \rightarrow \pi^*_y$	$\sigma^*_{x^2-y^2} \rightarrow \sigma^*_z$
Excited state	$(\sigma^*_{xy})^1(\sigma^*_{x^2-y^2})^2$	$(\sigma^*_{xy})^2(\pi^*_x)^1$	$(\sigma^*_{xy})^2(\pi^*_y)^1$	$(\sigma^*_{xy})^2(\sigma^*_z)^1$
4	4220	20020	22500	22280

1−3 feature a very low-lying excited state with an electron configuration of $(nb)^2(\pi^*_x)^1$, which lies above the ground state by only several hundred wavenumbers. Thus, complexes **1−3** possess an orbitally near degenerate ground state of effectively ^2E symmetry, consistent with the ligand field analysis. It should be noted that adjusting the Fe—N distance in the $(FeN)^{2+}$ core, the only geometric freedom of this moiety, cannot lift the double degeneracy of the two Fe—N π-bonds. Therefore, the small energy separation must arise from much weaker interactions between the iron center and the supporting ligand as found for **1−3**. The excitation energy of $\pi^*_y \rightarrow \sigma^*_z$ computed for **1** is much lower than those for **2** and **3**, mainly because the lack of a *trans* ligand in **1** stabilizes the σ_z^* orbital. In line with this reasoning, the Fe—nitrido bond length (1.56 Å) estimated for complex **1** is slightly shorter than those ($\sim$1.60 Å) for complexes **2** and **3**.

Complex **5** features a similar electronic structure as **1−3**, except for the considerably larger energy separation between the two components of ^2E. Furthermore, for complex **5**, the excitation energy of $\pi^*_y \rightarrow \sigma^*_{eq}$ was predicted to be much higher than that of $\pi^*_y \rightarrow \sigma^*_z$. This is due to the strong σ-donating capability of TAML, which raises the σ^*_{eq} orbital above σ^*_z.[52] The excitation from the nb d_{xy} orbital to the Fe—E π* orbital can be used to gauge the differential bonding strength between the iron-nitrido and -oxo π-interactions.[53] These excited states of complexes **1−3** were found to lie much higher in energy than that of **5**, thereby suggesting that the π-bond of iron(V)-nitrido complexes is substantially stronger than that of iron(V)-oxo species. For complexes **1** and **5**, both species featuring the same coordination geometry, our calculations showed that the excitation from π^*_y to the vacant σ^*_z orbital requires similar energy, although the π^*_y orbital of **1** is by far more destabilized than that of **5**. These findings show that iron(V)-nitrido complexes have stronger σ-bonds than iron(V)-oxo compounds. As a consequence, the iron-oxo interaction is more vulnerable to subtle perturbations. To test the ligand effect, we calculated the gap between the two components of the effective ^2E ground state of the hypothetical nitrido congener of **5**, $[Fe^V(N)(TAML)]^{2-}$ (**5-N**). The obtained value of 1000 cm⁻¹ is higher than those found for complexes **1−3** but lower than that for **5**. Therefore, not only the distinct iron(V)-nitrido and -oxo bonding strengths but also the strong donating capability of the TAML ligand lead to the larger energy separation for complex **5** compared to **1−3**. Because there are four negatively charged donors in TAML,

the gap estimated for **5** is probably close to the maximum value that can be reached in the iron(V)-nitrido and -oxo chemistry.

The differential bonding strength between the iron-nitrido and -oxo interactions explain why complex **1** features a distinctly different electronic structure compared to compound I. Our calculations show that, due to the much stronger iron-nitrido π-interactions, the two π^*_{Fe-N} orbitals (-3.8 eV) of the hypothetical one-electron reduced form of complex **1** are situated at higher energy than the porphyrin a_{1u} (-5.2 eV) and a_{2u} (-5.0 eV) orbitals (Figure S18). Consequently, the electron residing in the π^*_{Fe-N} orbital is more likely to be removed in the one-electron oxidation process. In other words, if a species formulated as $[Fe^{IV}(N)(TPP^{\bullet+})]^0$ were to be generated in the photolysis, the electron transfer from the singly occupied π^*_{Fe-N} orbitals to the vacant porphyrin π^*-orbital would have a tremendous driving force and would happen spontaneously. Further experimental investigations are required to verify this interpretation.

In agreement with an earlier study reported by Cutsail III et al.,[30] complex **4** has essentially an orbitally nondegenerate ground state with a leading electron configuration (78%) of $(\sigma^*_{xy})^2(\sigma^*_{x^2-y^2})^1$ (Figure S16). The considerably large energy gap (4220 cm^{-1}) of the two components of ^2E mainly results from the strong Jahn–Teller distortion in the equatorial plane, as evidenced by three distinct Fe—C bond lengths (1.932, 1.947, and 1.969 Å) shown in the crystal structure of **4**. As depicted in Figure S16, both σ^*_{xy} and $\sigma^*_{x^2-y^2}$ orbitals are essentially nonbonding in nature, because they contain predominant iron 3d character (94% and 84%, respectively) and rather limited C lone-pair character (<5%). The excitations of $\sigma^*_{x^2-y^2} \rightarrow \pi^*_{x/y}$ for complex **4** are, in fact, equivalent to those of nb$\rightarrow\pi^*_y$ for complexes **1–3**, because in both transitions one electron is promoted from the nb orbital to the Fe—N π^* orbital. These excitations of **1–4** were estimated to have comparable energy despite their different iron-nitrido bond orders. This observation is consistent with the notion that the SOMO ($\sigma^*_{x^2-y^2}$) of complex **4** is raised to higher energy due to the significant Jahn–Teller distortion. For complex **4**, the excitation energy of $\sigma^*_{x^2-y^2} \rightarrow \pi^*_{x/y}$ is comparable to that of $\sigma^*_{x^2-y^2} \rightarrow \sigma^*_z$, thereby suggesting that the π-bond in **4** is as strong as its σ-bond. This finding is due to the $3d_{z^2}$-$4s$-$4p_z$ mixing,[30] which significantly drops the energy of the σ_z^* orbital.

Ab Initio Calculations of the *g* Values of Iron(V)-Nitrido and -Oxo Complexes. The computed *g* values of complexes **1–5** by using CASSCF/NEVPT2 approach are summarized in Table 1. The theoretical results of complexes **1**, **4**, and **5** are in reasonable agreement with the experiment. However, for complexes **2** and **3**, our computations do not achieve quantitative agreement, especially for the lowest *g* components. Nevertheless, the estimated *g* values of complexes **1–3** and **5** reproduced the near-axial pattern with $g_\parallel < g_\perp \leq 2$ and the lowest *g* factors ($g_\parallel$) were found to align along the Fe—E bonds (Figure S22). For complex **4**, the largest *g* value was predicted along the Fe—N bond, and the other two are situated in the equatorial plane (Figure S22). In contrast to the ab initio results, the DFT computed *g* factors of complexes **1–3** and **5** are all very close to 2 (Table S1), further corroborating the notion that often DFT methods cannot be applied to orbitally near degenerate systems.

As discussed above, complexes **1–3** and **5** all possess a low-lying excited state. Thus, the large deviations of the estimated *g* values likely result from the error in the computed excitation

energy of this state. Taking complex **1** as an example, we examined its influence on the *g* values. In a series of five-root CASSCF/NEVPT2 calculations, we systematically varied the transition energy of $\pi^*_y \rightarrow \pi^*_x$ from 0 to 6000 cm^{-1} and kept the energy of other excited states fixed at the initially calculated values (Figure 5b). In parallel, we also carried out similar two-
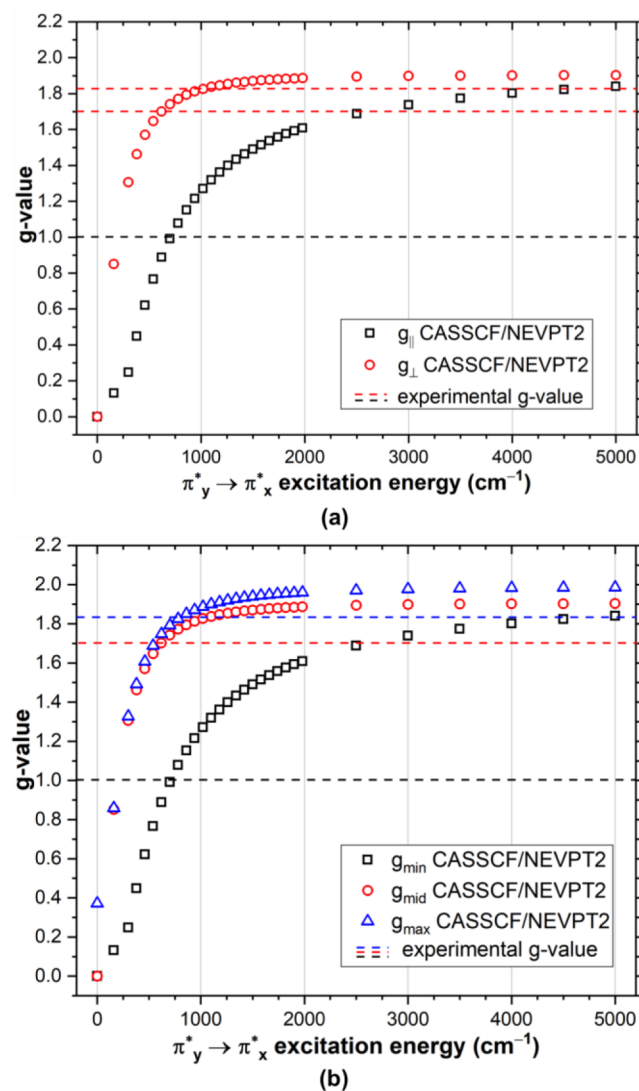

Figure 5. *g* values of complex **1** as a function of the excitation energy of $\pi^*_y \rightarrow \pi^*_x$ calculated by using CASSCF(11,12)/NEVPT2 calculations averaging two doublets (**a**) and five doublets (**b**). The experimental *g* values are denoted by dashed lines at $g = 1.00$, 1.70, and 1.83.

root CASSCF/NEVPT2 computations, where only the SOC of the effective ^2E ground state was taken into account (Figure 5a). The results obtained from both calculations are essentially identical. A similar behavior was also found for complex **2** (Figure S21). These findings suggest that the *g* values of complexes **1** and **2** are almost completely determined by the SOC between the two components of ^2E, which verifies the assumption of the ligand field model. Specifically, as the excitation energy changes from 0 to 3000 cm^{-1}, the $g_\parallel$ and $g_\perp$ values rocket from 0 to 1.8 and 2.0, respectively. As the excitation energy further increases, the $g_\parallel$ component slowly approaches to 2, while $g_\perp$ levels off at 2. Thus, the $g_\parallel$ value is

more sensitive to the variation of the excitation energy, because it gets saturated at higher excitation energy than $g_\perp$. To achieve better agreement with the experimental g values of complex **1** indicated by gray dashed lines in Figure 5, the excitation energy should be in the range of 600−800 cm^{-1}, at most 200 cm^{-1} above the calculated excitation energy (Table 2). This error is definitely beyond the accuracy of any quantum chemical calculations. Thus, our theoretical results clearly demonstrated that a minor change in the excitation energy of $\pi^*_y \rightarrow \pi^*_x$ has drastic influence on the g values, in particular $g_\parallel$. This explains the large error in the calculated g values of complexes **2** and **3**, because their first excited states are below 2500 cm^{-1}.

Given the electronic-structures of complexes **1**−**3** and **5**, we surmise that probably all tetragonal low spin iron(V)-nitrido and -oxo complexes feature effective ^{2}E ground states. Because of the exceedingly strong σ- and π-donating capability of the nitrido and oxo ligands, the overwhelming iron-nitrido and -oxo bonding overrides any other metal−ligand interactions, which in turn slightly lift the double degeneracy of ^{2}E. Bendix et al. proposed that the π^* orbitals in $[\text{Cr}^V(\text{N})\text{Cl}_4]^{2-}$ can be significantly destabilized and hence lie higher in energy than the σ^*_{eq} orbital.[54] Consequently, the classical 1−2−1−1 orbital splitting (Scheme 1a) does not hold true for $[\text{Cr}^V(\text{N})\text{Cl}_4]^{2-}$. Thus, one can envisage a ground-state electron configuration of $(\text{nb})^2(\sigma^*_{eq})^1$ for a low-spin iron(V)-nitrido and -oxo complex with a very weak equatorial coordination. To test this hypothesis, we computationally examined the corresponding hypothetical iron(V) complexes, $[\text{Fe}^V(\text{N})\text{Cl}_4]^{2-}$ and $[\text{Fe}^V(\text{O})\text{Cl}_4]^-$ (Figure S20). It turns out that both complexes feature qualitatively the same electronic structure as those found for complexes **1**−**3** and **5**. This finding further corroborates our proposed general bonding feature for tetragonal low spin iron(V)-nitrido and -oxo complexes. As a consequence, their EPR spectra would show a near-axial pattern with $g_\parallel$ considerably less than 2, and, more critically, the $g_\parallel$ and $g_\perp$ values fit eq 3, in analogy to those measured for complexes **1**−**3** and **5**.

Eq 3 has been shown to succeed in correlating the $g_\parallel$ and $g_\perp$ values of complexes **1**−**3** and **5**, because our numerical calculations revealed that the contributions from the higher lying excited states, other than the first excited state, to the g shifts are negligible (Figure 5). On the basis of the electronic structures found for complexes **1**−**3** and **5**, tetragonal low spin iron(V)-nitrido and -oxo complexes may be classified into two classes according to their equatorial coordination strength. On one hand, if complexes feature weak equatorial coordination, as exemplified by complexes **1**−**3**, they typically have a small energy gap of ~1000 cm^{-1} for the effective ^{2}E ground state. Their closely lying excited states likely arise from promoting the α-electron residing in the SOMO ($\pi^*_{\text{Fe-E}}$) to the equatorial σ-antibonding orbital (σ^*_{eq}). These excited states were computed to be situated at ~5000 cm^{-1} above the ground state for complexes **1**−**3**. Because the π-bonds of iron(V)-oxo complexes are much weaker than those of iron(V)-nitrido compounds, the corresponding excitations ($\pi^*_{\text{Fe-O}} \rightarrow \sigma^*_{eq}$) for iron(V)-oxo complexes should have much higher energy. On the other hand, if tetragonal low spin iron(V)-nitrido and -oxo complexes, such as **5**, are supported by very strong equatorial ligands, such systems often possess an energy separation of at most 2500 cm^{-1} for the effective ^{2}E ground state. However, different from the situation discussed above, the closely lying excited states probably originate from exciting the β-electron in

the doubly occupied nb orbitals to the SOMO ($\pi^*_{\text{Fe-E}}$). Our calculations on complexes **1**−**3** and **5** show the lower bound of the energy of these excited states is ~14000 cm^{-1}. Taken together, for both classes the energy of other excited states is at least four times higher than the energy separation of the effective ^{2}E ground state. Therefore, the in-state SOC essentially determines the g values of tetragonal iron(V)-nitrido and -oxo complexes, which provides a rationale for the general applicability of eq 3.

As elaborated in our earlier work,[22] complexes **6**, **7**, and **7-H**$^+$ feature different bonding situations from those found for **1**−**3** and **5**. As a consequence of their distinct electronic structures, the g values of **6**, **7**, and **7-H**$^+$ are all close to 2. More importantly, our theoretical studies revealed that complexes **5** and **5'** only can initiate one-electron chemistry, in agreement with experimental findings,[28] whereas **6** can function as a two-electron oxidant.[22] The reactions of C—H and C=C bond oxidation with complex **6** proceed without an intervening intermediate, which nicely explains the stereospecificity observed experimentally.

Recently, de Bruin and Schneider and co-workers reported synthesis and characterization of two pincer rhodium(IV)- and iridium(IV)-nitrido complexes, $[\text{RhN}\{\text{N}(\text{CHCHP}^t\text{Bu}_2)_2)\}]$ (**8**) and $[\text{IrN}\{\text{N}(\text{CHCHP}^t\text{Bu}_2)_2)\}]$ (**9**)[55] (Chart 3). Despite

Chart 3. Open-Shell Square Planar Nitrido Complexes
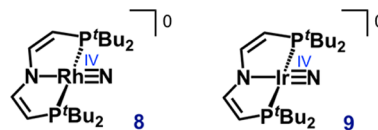
possessing a square planar coordination geometry, both complexes feature a similar electronic structure to those of **1**−**3** and **5** with a single electron occupied in the nearly degenerate $\pi^*_{\text{Rh/Ir}=\text{N}}$ orbitals. Unsurprisingly, their measured g values (for **8**, g = 2.04, 1.93, 1.70, and for **9**, g = 1.885, 1.631 and 1.320) also reasonably obey eq 3 (Figure 3), which provides an independent support for our proposed EPR signature of tetragonal low spin iron(V)-nitrido and -oxo complexes.

■ CONCLUSION

Our experimental and theoretical investigations evidence that complex **1**, a nitrido congener of compound I, is a bona fide low spin (S = 1/2) iron(V)-nitrido complex. The multi-reference CASSCF/NEVPT2 calculations revealed that tetragonal iron(V)-nitrido complexes **1**−**3** all feature a unique electronic structure having an orbitally near degenerate ground state with an electron configuration of $(\text{nb})^2(\pi^*_{\text{Fe-N}})^1$. A similar bonding situation was also found for tetragonal iron(V)-oxo complex **5**, but the gap between the two components of the effective ^{2}E ground state is larger. As a manifestation of their analogous electronic structures, their EPR spectra exhibit a near-axial pattern with $g_\parallel < g_\perp \leq 2$, and the lowest g component is considerably lower than 2. On the basis of their unique bonding features, a simple equation to correlate their $g_\parallel$ and $g_\perp$ values, $g_\perp^2 + (2 - g_\parallel)^2 = 4$, was derived. However, an electron configuration of $(\sigma^*_{xy})^2(\sigma^*_{x^2-y^2})^1$ was predicted for trigonal iron(V)-nitrido complex **4**, and due to strong Jahn−Teller distortions the system has essentially an orbitally nondegenerate ground state.

Consequently, complex **4** exhibits a distinct EPR spectrum with $g_\parallel < 2 < g_\perp$.

Further in-depth electronic-structure analysis suggested that tetragonal low spin iron(V)-nitrido and -oxo complexes possess electronic structures akin to those found for complexes **1**–**3** and **5**. Thus, the EPR signatures determined for complexes **1**–**3** and **5** can be used as a spectroscopic marker to identify analogous species in future studies.

This work provides deep insight into the electronic structures of iron(V)-nitrido and -oxo complexes, particularly in tetragonal coordination environments. The results should aid in detecting such important, yet usually short-lived, intermediates and understanding their functions in complex biological or industrial processes.

■ ASSOCIATED CONTENT

ⓢ Supporting Information

The Supporting Information is available free of charge on the ACS Publications website at DOI: 10.1021/jacs.8b11429.

> EPR spectra of azide precursors (**1^{pro}** and **2^{pro}**) and the samples after photolysis, Raman spectrum of photolyzed **1^{pro}**, Mössbauer spectrum of **1^{pro}**, the effect of the double d-shell on the ground state of complex **2**, CASSCF electronic structures of complexes **1**–**5**, key geometrical parameters of complexes **1**–**5** and the hypothetical complexes, dependence of g-tensors on the $\pi^*_y \rightarrow \pi^*_x$ excitation energy for complex **2**, orientation of the g matrices for complexes **1**–**5** (PDF)

■ AUTHOR INFORMATION

Corresponding Authors
*eckhard.bill@cec.mpg.de
*shengfa.ye@kofo.mpg.de

ORCID ⓘ
Hao-Ching Chang: 0000-0002-3479-094X
Bhaskar Mondal: 0000-0001-9026-5974
Huayi Fang: 0000-0002-8008-0383
Frank Neese: 0000-0003-4691-0547
Eckhard Bill: 0000-0001-9138-3964
Shengfa Ye: 0000-0001-9747-1412

Present Address
$^\perp$H.F.: Department of Chemistry, Fudan University, Shanghai 200433, China

Author Contributions
‡H.-C.C. and B.M. contributed equally to the present work.

Notes
The authors declare no competing financial interest.

■ ACKNOWLEDGMENTS

■ REFERENCES

(1) (a) Groves, J. T. High-valent iron in chemical and biological oxidations. *J. Inorg. Biochem.* **2006**, *100*, 434−447. (b) Hohenberger, J.; Ray, K.; Meyer, K. The biology and chemistry of high-valent iron−oxo and iron−nitrido complexes. *Nat. Commun.* **2012**, *3*, 720. (c) Cheng, J.; Wang, L.; Wang, P.; Deng, L. High-oxidation-state 3d metal (Ti−Cu) complexes with *N*-heterocyclic carbene ligation. *Chem. Rev.* **2018**, *118*, 9930−9987.

(2) (a) Tamanaha, E.; Zhang, B.; Guo, Y.; Chang, W.-C.; Barr, E. W.; Xing, G.; St Clair, J.; Ye, S.; Neese, F.; Bollinger, J. M., Jr; Krebs, C. Spectroscopic evidence for the two C−H-cleaving intermediates of *Aspergillus nidulans* isopenicillin N synthase. *J. Am. Chem. Soc.* **2016**, *138*, 8862−8874. (b) Krebs, C.; Galonić Fujimori, D.; Walsh, C. T.; Bollinger, J. M. Non-heme Fe(IV)−oxo intermediates. *Acc. Chem. Res.* **2007**, *40*, 484−492. (c) Krebs, C.; Price, J. C.; Baldwin, J.; Saleh, L.; Green, M. T.; Bollinger, J. M. Rapid freeze-quench ^{57}Fe Mössbauer spectroscopy: monitoring changes of an iron-containing active site during a biochemical reaction. *Inorg. Chem.* **2005**, *44*, 742−757. (d) Proshlyakov, D. A.; Henshaw, T. F.; Monterosso, G. R.; Ryle, M. J.; Hausinger, R. P. Direct detection of oxygen iIntermediates in the non-heme Fe enzyme taurine/α-ketoglutarate dioxygenase. *J. Am. Chem. Soc.* **2004**, *126*, 1022−1023. (e) Proshlyakov, D. A.; McCracken, J.; Hausinger, R. P. Spectroscopic analyses of 2-oxoglutarate-dependent oxygenases: TauD as a case study. *JBIC, J. Biol. Inorg. Chem.* **2017**, *22*, 367−379.

(3) (a) Solomon, E. I.; Brunold, T. C.; Davis, M. I.; Kemsley, J. N.; Lee, S.-K.; Lehnert, N.; Neese, F.; Skulan, A. J.; Yang, Y.-S.; Zhou, J. Geometric and electronic structure/function correlations in non-heme iron enzymes. *Chem. Rev.* **2000**, *100*, 235−350. (b) Costas, M.; Mehn, M. P.; Jensen, M. P.; Que, L., Jr. Dioxygen activation at mononuclear nonheme iron active sites: enzymes, models, and intermediates. *Chem. Rev.* **2004**, *104*, 939−986. (c) McDonald, A. R.; Que, L., Jr. High-valent nonheme iron-oxo complexes: synthesis, structure, and spectroscopy. *Coord. Chem. Rev.* **2013**, *257*, 414−428. (d) Nam, W. High-valent iron(IV)-oxo complexes of heme and non-heme ligands in oxygenation reactions. *Acc. Chem. Res.* **2007**, *40*, 522−531.

(4) (a) Wang, Y.; Li, J.; Liu, A. Oxygen activation by mononuclear nonheme iron dioxygenases involved in the degradation of aromatics. *JBIC, J. Biol. Inorg. Chem.* **2017**, *22*, 395−405. (b) Ferraro, D. J.; Gakhar, L.; Ramaswamy, S. Rieske business: structure-function of Rieske non-heme oxygenases. *Biochem. Biophys. Res. Commun.* **2005**, *338*, 175−190. (c) Wolfe, M. D.; Lipscomb, J. D. Hydrogen peroxide-coupled *cis*-diol formation catalyzed by naphthalene 1,2-dioxygenase. *J. Biol. Chem.* **2003**, *278*, 829−835. (d) Kovaleva, E. G.; Lipscomb, J. D. Versatility of biological non-heme Fe(II) centers in oxygen activation reactions. *Nat. Chem. Biol.* **2008**, *4*, 186−193. (e) Barry, S. M.; Challis, G. L. Mechanism and catalytic diversity of Rieske non-heme iron-dependent oxygenases. *ACS Catal.* **2013**, *3*, 2362−2370.

(5) (a) *The Porphyrin Handbook, Vol. 4/Biochemistry and binding: activation of small molecules*; Kadish, K. M., Smith, K. M., Guilard, R., Eds.; Academic Press: San Diego, CA, 2000. (b) *Cytochrome P450: structure, mechanism, and biochemistry*, 4th ed.; Ortiz de Montellano, P. R., Ed.; Springer International Publishing: Switzerland, 2015. (c) Poulos, T. L. Heme enzyme structure and function. *Chem. Rev.* **2014**, *114*, 3919−3962. (d) Sono, M.; Roach, M. P.; Coulter, E. D.; Dawson, J. H. Heme-containing oxygenases. *Chem. Rev.* **1996**, *96*, 2841−2887. (e) Monooxygenase, peroxidase and peroxygenase properties and reaction mechanisms of cytochrome P450 enzymes; Hrycay, E. G., Bandiera, S. M., Eds.; Springer International Publishing: Switzerland, 2015; pp 1−61. (f) Jung, C. The mystery of cytochrome P450 compound I, a mini-review dedicated to Klaus Ruckpaul. *Biochim. Biophys. Acta, Proteins Proteomics* **2011**, *1814*, 46−57. (g) Fujii, H. Electronic structure and reactivity of high-valent oxo iron porphyrins. *Coord. Chem. Rev.* **2002**, *226*, 51−60.

(6) Moss, T. H.; Ehrenberg, A.; Bearden, A. J. Mössbauer spectroscopic evidence for the electronic configuration of iron in horseradish peroxidase and its peroxide derivatives. *Biochemistry* **1969**, *8*, 4159−4162.

(7) (a) Schulz, C. E.; Rutter, R.; Sage, J. T.; Debrunner, P. G.; Hager, L. P. Mössbauer and electron paramagnetic resonance studies of horseradish peroxidase and its catalytic intermediates. *Biochemistry* **1984**, *23*, 4743−4754. (b) Rutter, R.; Hager, L. P.; Dhonau, H.; Hendrich, M.; Valentine, M.; Debrunner, P. Chloroperoxidase compound I: Electron paramagnetic resonance and Mössbauer

studies. *Biochemistry* **1984**, *23*, 6809−6816. (c) Rittle, J.; Green, M. T. Cytochrome P450 compound I: capture, characterization, and C−H bond activation kinetics. *Science* **2010**, *330*, 933−937.

(8) (a) Boso, B.; Lang, G.; McMurry, T. J.; Groves, J. T. Mössbauer effect study of tight spin coupling in oxidized chloro-5,10,15,20-tetra(mesityl)porpyhrinatoiron(III). *J. Chem. Phys.* **1983**, *79*, 1122−1126. (b) Mandon, D.; Weiss, R.; Jayaraj, K.; Gold, A.; Terner, J.; Bill, E.; Trautwein, A. X. Models for peroxidase compound I: generation and spectroscopic characterization of new oxoferryl porphyrin π-cation radical species. *Inorg. Chem.* **1992**, *31*, 4404−4409. (c) Jayaraj, K.; Gold, A.; Austin, R. N.; Mandon, D.; Weiss, R.; Terner, J.; Bill, E.; Müther, M.; Trautwein, A. X. Compound-I and Compound-II Analogs of a Chlorin. *J. Am. Chem. Soc.* **1995**, *117*, 9079−9080. (d) Jayaraj, K.; Gold, A.; Austin, R. N.; Ball, L. M.; Terner, J.; Mandon, D.; Weiss, R.; Fischer, J.; DeCian, A.; Bill, E.; Müther, M.; Schünemann, V.; Trautwein, A. X. Compound I and compound II analogues from porpholactones. *Inorg. Chem.* **1997**, *36*, 4555−4566. (e) Fujita, I.; Hanson, L. K.; Walker, F. A.; Fajer, J. Models for compounds I of peroxidases: axial ligand effects. *J. Am. Chem. Soc.* **1983**, *105*, 3296−3300. (f) Huang, X.; Groves, J. T. Oxygen Activation and Radical Transformations in Heme Proteins and Metalloporphyrins. *Chem. Rev.* **2018**, *118*, 2491−2553.

(9) (a) Mehn, M. P.; Peters, J. C. Mid- to high-valent imido and nitrido complexes of iron. *J. Inorg. Biochem.* **2006**, *100*, 634−643. (b) Saouma, C. T.; Peters, J. C. M≡E and M = E complexes of iron and cobalt that emphasize three-fold symmetry (E = O, N, NR). *Coord. Chem. Rev.* **2011**, *255*, 920−937. (c) Berry, J. F. Terminal nitrido and imido complexes of the late transition metals. *Comments Inorg. Chem.* **2009**, *30*, 28−66. (d) Smith, J. M.; Subedi, D. The structure and reactivity of iron nitride complexes. *Dalton Trans.* **2012**, *41*, 1423−1429. (e) Smith, J. M. Reactive transition metal nitride complexes. *Prog. Inorg. Chem.* **2014**, *58*, 417−470.

(10) (a) Fryzuk, M. D.; Johnson, S. A. The continuing story of dinitrogen activation. *Coord. Chem. Rev.* **2000**, *200−202*, 379−409. (b) MacKay, B. A.; Fryzuk, M. D. Dinitrogen coordination chemistry: on the biomimetic borderlands. *Chem. Rev.* **2004**, *104*, 385−402.

(11) (a) Wagner, W. D.; Nakamoto, K. Formation of nitridoiron(V) porphyrins detected by resonance Raman spectroscopy. *J. Am. Chem. Soc.* **1988**, *110*, 4044−4045. (b) Wagner, W.-D.; Nakamoto, K. Resonance Raman spectra of nitridoiron(V) porphyrin intermediates produced by laser photolysis. *J. Am. Chem. Soc.* **1989**, *111*, 1590−1598.

(12) Czernuszewicz, R. S.; Su, Y. O.; Stern, M. K.; Macor, K. A.; Kim, D.; Groves, J. T.; Spiro, T. G. Oxomanganese(IV) porphyrins identified by resonance Raman and infrared spectroscopy. Weak bonds and the stability of the half-filled t_{2g} subshell. *J. Am. Chem. Soc.* **1988**, *110*, 4158−4165.

(13) (a) Grapperhaus, C. A.; Mienert, B.; Bill, E.; Weyhermüller, T.; Wieghardt, K. Mononuclear (nitrido)iron(V) and (oxo)iron(IV) complexes via photolysis of [(cyclam-acetato)Fe^{III}(N$_3$)]$^+$ and ozonolysis of [(cyclam-acetato)Fe^{III}(O$_3$SCF$_3$)]$^+$ in water/acetone mixtures. *Inorg. Chem.* **2000**, *39*, 5306−5317. (b) Aliaga-Alcalde, N.; DeBeer George, S.; Mienert, B.; Bill, E.; Wieghardt, K.; Neese, F. The geometric and electronic structure of [(cyclam-acetato)Fe(N)]$^+$: a genuine iron(V) species with a ground-state spin S = 1/2. *Angew. Chem., Int. Ed.* **2005**, *44*, 2908−2912. (c) Petrenko, T.; DeBeer George, S.; Aliaga-Alcalde, N.; Bill, E.; Mienert, B.; Xiao, Y.; Guo, Y.; Sturhahn, W.; Cramer, S. P.; Wieghardt, K.; Neese, F. Characterization of a genuine iron(V)-nitrido species by nuclear resonant vibrational spectroscopy coupled to density functional calculations. *J. Am. Chem. Soc.* **2007**, *129*, 11053−11060.

(14) Krahe, O. Experimental and theoretical studies of mononuclear high-valent nitrido-iron and oxo-iron complexes. Ph.D. Thesis, University of Bonn, April 2016.

(15) Meyer, K.; Bill, E.; Mienert, B.; Weyhermüller, T.; Wieghardt, K. Photolysis of *cis-* and *trans-*[Fe^{III}(cyclam)(N$_3$)$_2$]$^+$ complexes: spectroscopic characterization of a nitridoiron(V) species. *J. Am. Chem. Soc.* **1999**, *121*, 4859−4876.

(16) (a) Sabenya, G.; Lázaro, L.; Gamba, I.; Martin-Diaconescu, V.; Andris, E.; Weyhermüller, T.; Neese, F.; Roithová, J.; Bill, E.; Lloret-Fillol, J.; Costas, M. Generation, spectroscopic, and chemical characterization of an octahedral iron(V)-nitrido species with a neutral ligand platform. *J. Am. Chem. Soc.* **2017**, *139*, 9168−9177. (b) Andris, E.; Navrátil, R.; Jašík, J.; Sabenya, G.; Costas, M.; Srnec, M.; Roithová, J. Detection of indistinct Fe−N stretching bands in iron(V) nitrides by photodissociation spectroscopy. *Chem. - Eur. J.* **2018**, *24*, 5078−5081.

(17) Schlangen, M.; Neugebauer, J.; Reiher, M.; Schröder, D.; López, J. P.; Haryono, M.; Heinemann, F. W.; Grohmann, A.; Schwarz, H. Gas-phase C−H and N−H bond activation by a high valent nitrido-iron dication and < NH>-transfer to activated olefins. *J. Am. Chem. Soc.* **2008**, *130*, 4285−4294.

(18) Scepaniak, J. J.; Vogel, C. S.; Khusniyarov, M. M.; Heinemann, F. W.; Meyer, K.; Smith, J. M. Synthesis, structure, and reactivity of an iron(V) nitride. *Science* **2011**, *331*, 1049−1052.

(19) de Oliveira, F. T.; Chanda, A.; Banerjee, D.; Shan, X.; Mondal, S.; Que, L., Jr.; Bominaar, E. L.; Münck, E.; Collins, T. J. Chemical and spectroscopic evidence for an Fe^V-oxo complex. *Science* **2007**, *315*, 835−838.

(20) (a) Ghosh, M.; Singh, K. K.; Panda, C.; Weitz, A.; Hendrich, M. P.; Collins, T. J.; Dhar, B. B.; Sen Gupta, S. Formation of a room temperature stable Fe^V(O) complex: reactivity toward unactivated C−H bonds. *J. Am. Chem. Soc.* **2014**, *136*, 9524−9527. (b) Mills, M. R.; Weitz, A. C.; Hendrich, M. P.; Ryabov, A. D.; Collins, T. J. NaClO-generated iron(IV)oxo and iron(V)oxo TAMLs in pure water. *J. Am. Chem. Soc.* **2016**, *138*, 13866−13869.

(21) (a) Serrano-Plana, J.; Oloo, W. N.; Acosta-Rueda, L.; Meier, K. K.; Verdejo, B.; García-España, E.; Basallote, M. G.; Münck, E.; Que, L., Jr.; Company, A.; Costas, M. Trapping a highly reactive nonheme iron intermediate that oxygenates strong C−H bonds with stereo-retention. *J. Am. Chem. Soc.* **2015**, *137*, 15833−15842. (b) Fan, R.; Serrano-Plana, J.; Oloo, W. N.; Draksharapu, A.; Delgado-Pinar, E.; Company, A.; Martin-Diaconescu, V.; Borrell, M.; Lloret-Fillol, J.; García-España, E.; Guo, Y.; Bominaar, E. L.; Que, L., Jr.; Costas, M.; Münck, E. Spectroscopic and DFT characterization of a highly reactive nonheme Fe^V−oxo intermediate. *J. Am. Chem. Soc.* **2018**, *140*, 3916−3928. (c) Olivo, G.; Cussó, O.; Borrell, M.; Costas, M. Oxidation of alkane and alkene moieties with biologically inspired nonheme iron catalysts and hydrogen peroxide: from free radicals to stereoselective transformations. *JBIC, J. Biol. Inorg. Chem.* **2017**, *22*, 425−452. (d) Zhang, J.; Wei, W.-J.; Lu, X.; Yang, H.; Chen, Z.; Liao, R.-Z.; Yin, G. Nonredox metal ions promoted olefin epoxidation by iron(II) complexes with H$_2$O$_2$: DFT calculations reveal multiple channels for oxygen transfer. *Inorg. Chem.* **2017**, *56*, 15138−15149. (e) Oloo, W. N.; Que, L., Jr. Bioinspired nonheme iron catalysts for C−H and C═C bond oxidation: insights into the nature of the metal-based oxidants. *Acc. Chem. Res.* **2015**, *48*, 2612−2621. (f) Sun, C.-L.; Li, B.-J.; Shi, Z.-J. Direct C−H transformation *via* iron catalysis. *Chem. Rev.* **2011**, *111*, 1293−1314. (g) Lyakin, O. Y.; Bryliakov, K. P.; Britovsek, G. J. P.; Talsi, E. P. EPR spectroscopic trapping of the active species of nonheme iron-catalyzed oxidation. *J. Am. Chem. Soc.* **2009**, *131*, 10798−10799. (h) Chen, M. S.; White, M. C. A predictably selective aliphatic C-H oxidation reaction for complex molecule synthesis. *Science* **2007**, *318*, 783−787. (i) Chen, M. S.; White, M. C. Combined effects on selectivity in Fe-catalyzed methylene oxidation. *Science* **2010**, *327*, 566−571.

(22) Mondal, B.; Neese, F.; Bill, E.; Ye, S. Electronic structure contributions of non-heme oxo-iron(V) complexes to the reactivity. *J. Am. Chem. Soc.* **2018**, *140*, 9531−9544.

(23) Van Heuvelen, K. M.; Fiedler, A. T.; Shan, X.; De Hont, R. F.; Meier, K. K.; Bominaar, E. L.; Münck, E.; Que, L., Jr. One-electron oxidation of an oxoiron (IV) complex to form an [O═Fe^V═NR]$^+$ center. *Proc. Natl. Acad. Sci. U. S. A.* **2012**, *109*, 11933−11938.

(24) Summerville, D. A.; Cohen, I. A. Metal-metal interactions involving metalloporphyrins. III. Conversion of tetraphenylporphinatoiron(III) azide to an N-bridged hemin dimer. *J. Am. Chem. Soc.* **1976**, *98*, 1747−1752.

(25) Krahe, O.; Bill, E.; Neese, F. Decay of iron(V) nitride complexes by a N–N bond-coupling reaction in solution: a combined spectroscopic and theoretical analysis. *Angew. Chem., Int. Ed.* **2014**, *53*, 8727–8731.

(26) Schröder, D.; Schwarz, H.; Aliaga-Alcalde, N.; Neese, F. Fragmentation of the (cyclam-acetato)iron azide cation in the gas phase. *Eur. J. Inorg. Chem.* **2007**, *2007*, 816–821.

(27) (a) Torres-Alacan, J.; Krahe, O.; Filippou, A. C.; Neese, F.; Schwarzer, D.; Vöhringer, P. The photochemistry of [Fe^{III}N$_3$(cyclam-ac)]PF$_6$ at 266 nm. *Chem. - Eur. J.* **2012**, *18*, 3043–3055. (b) Torres-Alacan, J.; Das, U.; Filippou, A. C.; Vöhringer, P. C Observing the formation and the reactivity of an octahedral iron(V) nitrido complex in real time. *Angew. Chem., Int. Ed.* **2013**, *52*, 12833–12837.

(28) (a) Kundu, S.; Thompson, J. V. K.; Shen, L. Q.; Mills, M. R.; Bominaar, E. L.; Ryabov, A. D.; Collins, T. J. Activation parameters as mechanistic probes in the TAML iron(V)-oxo oxidations of hydrocarbons. *Chem. - Eur. J.* **2015**, *21*, 1803–1810. (b) Kundu, S.; Thompson, J. V. K.; Ryabov, A. D.; Collins, T. J. On the reactivity of mononuclear iron(V)oxo complexes. *J. Am. Chem. Soc.* **2011**, *133*, 18546–18549. (c) Kwon, E.; Cho, K.-B.; Hong, S.; Nam, W. Mechanistic insight into the hydroxylation of alkanes by a nonheme iron(V)-oxo complex. *Chem. Commun.* **2014**, *50*, 5572–5575. (d) Collins, T. J.; Ryabov, A. D. Targeting of high-valent iron-TAML activators at hydrocarbons and beyond. *Chem. Rev.* **2017**, *117*, 9140–9162.

(29) Panda, C.; Debgupta, J.; Díaz, D. D.; Singh, K. K.; Gupta, S. S.; Dhar, B. B. Homogeneous photochemical water oxidation by biuret-modified Fe-TAML: evidence of Fe^V(O) intermediate. *J. Am. Chem. Soc.* **2014**, *136*, 12273–12282.

(30) Cutsail, G. E., III; Stein, B. W.; Subedi, D.; Smith, J. M.; Kirk, M. L.; Hoffman, B. M. EPR, ENDOR, and electronic structure studies of the Jahn–Teller distortion in an Fe^V nitride. *J. Am. Chem. Soc.* **2014**, *136*, 12323–12336.

(31) Adams, K. M.; Rasmussen, P. G.; Scheidt, W. R.; Hatano, K. Structure and properties of an unsymmetrically substituted six-coordinate iron(III) porphyrin. *Inorg. Chem.* **1979**, *18*, 1892–1899.

(32) Aasa, R.; Vänngård, T. EPR signal intensity and powder shapes: a reexamination. *J. Magn. Reson.* **1975**, *19*, 308–315.

(33) Neese, F. Software update: the ORCA program system, version 4.0. *WIREs Comput. Mol. Sci.* **2018**, *8*, e1327.

(34) (a) Becke, A. D. Density-functional exchange-energy approximation with correct asymptotic behavior. *Phys. Rev. A: At., Mol., Opt. Phys.* **1988**, *38*, 3098–3100. (b) Perdew, J. P. Density-functional approximation for the correlation energy of the inhomogeneous electron gas. *Phys. Rev. B: Condens. Matter Mater. Phys.* **1986**, *33*, 8822–8824. (c) Perdew, J. P. Erratum: Density-functional approximation for the correlation energy of the inhomogeneous electron gas. *Phys. Rev. B: Condens. Matter Mater. Phys.* **1986**, *34*, 7406.

(35) Vahtras, O.; Almlöf, J.; Feyereisen, M. W. Integral approximations for LCAO-SCF calculations. *Chem. Phys. Lett.* **1993**, *213*, 514–518.

(36) (a) Schafer, A.; Horn, H.; Ahlrichs, R. Fully optimized contracted Gaussian basis sets for atoms Li to Kr. *J. Chem. Phys.* **1992**, *97*, 2571–2577. (b) Weigend, F.; Ahlrichs, R. Balanced basis sets of split valence, triple zeta valence and quadruple zeta valence quality for H to Rn: Design and assessment of accuracy. *Phys. Chem. Chem. Phys.* **2005**, *7*, 3297–3305.

(37) Tomasi, J.; Mennucci, B.; Cammi, R. Quantum mechanical continuum solvation models. *Chem. Rev.* **2005**, *105*, 2999–3094.

(38) (a) Roos, B. O. The complete active space self-consistent field method and its applications in electronic structure calculations. *Adv. Chem. Phys.* **2007**, *69*, 399–445. (b) Ruedenberg, K.; Cheung, L. M.; Elbert, S. T. MCSCF optimization through combined use of natural orbitals and the Brillouin–Levy–Berthier theorem. *Int. J. Quantum Chem.* **1979**, *16*, 1069–1101. (c) Roos, B. O.; Taylor, P. R.; Siegbahn, P. E. M. A complete active space SCF method (CASSCF) using a density matrix formulated super-CI approach. *Chem. Phys.* **1980**, *48*, 157–173.

(39) (a) Angeli, C.; Borini, S.; Cestari, M.; Cimiraglia, R. A quasidegenerate formulation of the second order n-electron valence state perturbation theory approach. *J. Chem. Phys.* **2004**, *121*, 4043–4049. (b) Angeli, C.; Cimiraglia, R.; Malrieu, J.-P. N-electron valence state perturbation theory: a spinless formulation and an efficient implementation of the strongly contracted and of the partially contracted variants. *J. Chem. Phys.* **2002**, *117*, 9138–9153.

(40) (a) Neese, F.; Petrenko, T.; Ganyushin, D.; Olbrich, G. Advanced aspects of *ab initio* theoretical optical spectroscopy of transition metal complexes: multiplets, spin-orbit coupling and resonance Raman intensities. *Coord. Chem. Rev.* **2007**, *251*, 288–327. (b) Ganyushin, D.; Neese, F. A fully variational spin-orbit coupled complete active space self-consistent field approach: application to electron paramagnetic resonance g-tensors. *J. Chem. Phys.* **2013**, *138*, 104113.

(41) (a) Gerloch, M.; McMeeking, R. F. Paramagnetic properties of unsymmetrical transition-metal complexes. *J. Chem. Soc., Dalton Trans.* **1975**, 2443–2451. (b) Bolvin, H. An alternative approach to the g-matrix: theory and applications. *ChemPhysChem* **2006**, *7*, 1575–1589. (c) Chibotaru, L. F.; Ungur, L. *Ab initio* calculation of anisotropic magnetic properties of complexes. I. Unique definition of pseudospin Hamiltonians and their derivation. *J. Chem. Phys.* **2012**, *137*, 064112.

(42) (a) Ye, S.; Bill, E.; Neese, F. Electronic structures of the [Fe(N$_2$)(SiP$^{iPr}_3$)]$^{+1/0/−1}$ electron transfer series: a counterintuitive correlation between isomer shifts and oxidation states. *Inorg. Chem.* **2016**, *55*, 3468–3474. (b) Ye, S.; Neese, F. The unusual electronic structure of dinitrosyl iron complexes. *J. Am. Chem. Soc.* **2010**, *132*, 3646–3647. (c) Neese, F. Prediction and interpretation of the ^{57}Fe isomer shift in Mössbauer spectra by density functional theory. *Inorg. Chim. Acta* **2002**, *337*, 181–182.

(43) Andris, E.; Navrátil, R.; Jasík, J.; Sabenya, G.; Costas, M.; Srnec, M.; Roithová, J. Spin-state-controlled photodissociation of iron(III) azide to an iron(V) nitride complex. *Angew. Chem., Int. Ed.* **2017**, *56*, 14057–14060.

(44) (a) Mondal, B.; Roy, L.; Neese, F.; Ye, S. High-valent iron-oxo and -nitrido complexes: bonding and reactivity. *Isr. J. Chem.* **2016**, *56*, 763–772. (b) Ye, S.; Geng, C.-Y.; Shaik, S.; Neese, F. Electronic structure analysis of multistate reactivity in transition metal catalyzed reactions: the case of C–H bond activation by non-heme iron(IV)–oxo cores. *Phys. Chem. Chem. Phys.* **2013**, *15*, 8017–8030. (c) Geng, C.; Ye, S.; Neese, F. Does a higher metal oxidation state necessarily imply higher reactivity toward H-atom transfer? A computational study of C–H bond oxidation by high-valent iron-oxo and -nitrido complexes. *Dalton Trans.* **2014**, *43*, 6079–6086.

(45) (a) Ballhausen, C. J.; Gray, H. B. The electronic structure of the vanadyl ion. *Inorg. Chem.* **1962**, *1*, 111–122. (b) Nugent, W. A.; Mayer, J. M. *Metal-ligand multiple bonds: the chemistry of transition metal complexes containing oxo, nitrido, imido, alkylidene, or alkylidyne ligands*; John Wiley & Sons: New York, pp 33–36.

(46) Maity, A. K.; Murillo, J.; Metta-Magaña, A. J.; Pinter, B.; Fortier, S. A Terminal iron(IV) nitride supported by a super bulky guanidinate ligand and examination of its electronic structure and reactivity. *J. Am. Chem. Soc.* **2017**, *139*, 15691–15700.

(47) (a) Neese, F.; Solomon, E. I. Calculation of zero-field splittings, g-values, and the relativistic nephelauxetic effect in transition metal complexes. Application to high-spin ferric complexes. *Inorg. Chem.* **1998**, *37*, 6568–6582. (b) Mabbs, F. E.; Collison, D. *Electron Paramagnetic Resonance of d Transition Metal Compounds*; Mabbs, F. E., Collison, D., Eds.; Elsevier Science: Amsterdam, 1992; p 17. (c) Atherton, N. M. *Principles of Electron Spin Resonance*; Ellis Horwood Limited: Chichester, West Sussex, England, 1993. (d) Weil, J. A.; Bolton, J. R. *Electron Paramagnetic Resonance - Elementary Theory and Practical Applications*; John Wiley & Sons, Inc: Hoboken, NJ, 2007. (e) Carrington, A.; McLachlan, A. D. *Introduction to Magnetic Resonance*; Harper & Row John Weatherhill: New York/Tokyo, 1969.

(48) Bendix, J.; Brorson, M.; Schaffer, C. E. Accurate empirical spin-orbit coupling parameters ζ_{nd} for gaseous nd^q transition metal ions.

The parametrical multiplet term model. *Inorg. Chem.* **1993**, *32*, 2838–2849.

(49) Neese, F. Prediction of molecular properties and molecular spectroscopy with density functional theory: From fundamental theory to exchange-coupling. *Coord. Chem. Rev.* **2009**, *253*, 526–563.

(50) (a) Kupper, C.; Mondal, B.; Serrano-Plana, J.; Klawitter, I.; Neese, F.; Costas, M.; Ye, S.; Meyer, F. Nonclassical single-state reactivity of an oxo-iron(IV) complex confined to triplet pathways. *J. Am. Chem. Soc.* **2017**, *139*, 8939–8949. (b) Ye, S.; Kupper, C.; Meyer, S.; Andris, E.; Navrátil, R.; Krahe, O.; Mondal, B.; Atanasov, M.; Bill, E.; Roithová, J.; Meyer, F.; Neese, F. Magnetic circular dichroism evidence for an unusual electronic structure of a tetracarbene-oxoiron(IV) complex. *J. Am. Chem. Soc.* **2016**, *138*, 14312–14325. (c) Ye, S.; Xue, G.; Krivokapic, I.; Petrenko, T.; Bill, E.; Que, L., Jr; Neese, F. Magnetic circular dichroism and computational study of mononuclear and dinuclear iron(IV) complexes. *Chem. Sci.* **2015**, *6*, 2909–2921.

(51) Berry, J. F.; DeBeer George, S.; Neese, F. Electronic structure and spectroscopy of "superoxidized" iron centers in model systems: theoretical and experimental trends. *Phys. Chem. Chem. Phys.* **2008**, *10*, 4361–4374.

(52) Chanda, A.; Shan, X.; Chakrabarti, M.; Ellis, W. C.; Popescu, D. L.; Tiago de Oliveira, F.; Wang, D.; Que, L., Jr.; Collins, T. J.; Münck, E.; Bominaar, E. L. (TAML)Fe^{IV}=O complex in aqueous solution: synthesis and spectroscopic and computational characterization. *Inorg. Chem.* **2008**, *47*, 3669–3678.

(53) Decker, A.; Rohde, J.-U.; Klinker, E. J.; Wong, S. D.; Que, L., Jr.; Solomon, E. I. Spectroscopic and quantum chemical studies on low-spin Fe^{IV}=O complexes: Fe–O bonding and its contributions to reactivity. *J. Am. Chem. Soc.* **2007**, *129*, 15983–15996.

(54) Bendix, J. [Cr(N)Cl$_4$]$^{2-}$: a simple nitrido complex synthesized by nitrogen-atom transfer. *J. Am. Chem. Soc.* **2003**, *125*, 13348–13349.

(55) (a) Scheibel, M. G.; Wu, Y.; Stückl, A. C.; Krause, L.; Carl, E.; Stalke, D.; de Bruin, B.; Schneider, S. Synthesis and reactivity of a transient, terminal nitrido complex of rhodium. *J. Am. Chem. Soc.* **2013**, *135*, 17719–17722. (b) Scheibel, M. G.; Askevold, B.; Heinemann, F. W.; Reijerse, E. J.; de Bruin, B.; Schneider, S. Closed-shell and open-shell square-planar iridium nitrido complexes. *Nat. Chem.* **2012**, *4*, 552–558.